

NASA CONTRACTOR REPORT



NASA CR-12

0060586

TECH LIBRARY KAFB, NM

NASA CR-1273

LOAN COPY: RETURN TO
AFWL (WLIL-2)
KIRTLAND AFB, N MEX

IMPROVEMENT OF AN INTEGRAL EQUATION METHOD IN PLANE ELASTICITY THROUGH MODIFICATION OF SOURCE DENSITY REPRESENTATION

by Kwan Rim and Allen S. Henry

Prepared by
UNIVERSITY OF IOWA
Iowa City, Iowa
for

NATIONAL AERONAUTICS AND SPACE ADMINISTRATION • WASHINGTON, D. C. • FEBRUARY 1969



IMPROVEMENT OF AN INTEGRAL EQUATION METHOD IN PLANE ELASTICITY
THROUGH MODIFICATION OF SOURCE DENSITY REPRESENTATION

By Kwan Rim and Allen S. Henry

Distribution of this report is provided in the interest of
information exchange. Responsibility for the contents
resides in the author or organization that prepared it.

Prepared under Grant No. NsG-576 by
UNIVERSITY OF IOWA
Iowa City, Iowa

for

NATIONAL AERONAUTICS AND SPACE ADMINISTRATION



TABLE OF CONTENTS

<u>SECTION</u>	<u>PAGE</u>
SUMMARY	1
INTRODUCTION	1
THE INTEGRAL EQUATION METHOD	3
CONSIDERATION OF SOURCE DENSITY CONTINUITY	5
REPRESENTATION OF THE SOURCE DENSITY FUNCTIONS	8
REPRESENTATIONS FOR BOUNDARY STRESSES	11
BOUNDARY APPROXIMATIONS AND LIMIT FORMULAS	12
NUMERICAL CALCULATION OF BOUNDARY STRESSES	17
Evaluation of I^{ρ} , I_{ϵ}^{ρ} , I_{η}^{ρ} , $I_{\epsilon\epsilon}^{\rho}$, and $I_{\eta\epsilon}^{\rho}$	17
Integration over Intervals $i-1$ and $i+2$	18
Summary of the Computational Technique	20
NUMERICAL EXAMPLES	21
Discussion of Results for the Ellipse with $a/b = 2$	21
Discussion of Results for the Ellipse with $a/b = 5$	29
General Comments on the Numerical Results	34
CONCLUDING REMARKS	35
APPENDIX A DERIVATION OF LIMIT FORMULAS	36
REFERENCES	43



LIST OF SYMBOLS

D	planar domain.
L	closed curve of length $ L $, a boundary of D.
P	vector point in D at (x, y) .
p	vector point on L at (x, y) .
q	vector point on L with coordinates (x_q, y_q) .
\bar{n}, \bar{s}	unit vectors normal and tangent respectively to L.
n, s	coordinates measured in the direction of \bar{n} and \bar{s} respectively.
ϵ, η	rectangular coordinates measured in the direction of \bar{n} and \bar{s} with origin at p on L.
χ	stress function biharmonic in D.
ϕ, ψ	harmonic functions in D.
$\log P-q $	the natural logarithm of the scalar distance between $P(x, y)$ and $q(x, y)$.
$\sigma_x, \sigma_y, \tau_{xy}$	stress components.
σ_t, τ_t	normal and shear stress components tangent to L at p.
σ_n	normal stress component perpendicular to L at p.
θ	total stress, $\theta = \sigma_x + \sigma_y = \sigma_n + \sigma_t$.
F_x, F_y	x- and y- components of the stress vector on L.
∇^2	Laplace's operator $\nabla^2 = \frac{\partial^2}{\partial x^2} + \frac{\partial^2}{\partial y^2}$.
σ, μ, ρ	source densities defined on L.
a, b	semi-major and semi-minor axes of an ellipse.
$f'(p)$	$\frac{df}{dn}$ evaluated at p.

IMPROVEMENT OF AN INTEGRAL EQUATION METHOD IN PLANE ELASTICITY
THROUGH MODIFICATION OF SOURCE DENSITY REPRESENTATION

By Kwan Rim and Allen S. Henry

Department of Mechanics and Hydraulics
The University of Iowa
Iowa City, Iowa

SUMMARY

This report is a sequel to the work presented by the authors in "An Integral Equation Method in Plane Elasticity," NASA Contractor Report, NASA CR-779. The preceding report presented numerical results obtained from a formulation of the biharmonic stress function for the first fundamental boundary-value problem in plane elastostatics in terms of two single-layer potentials, each containing an unknown source density function.

The research reported herein shows that greater accuracy in calculated boundary stress components can be obtained if the numerically-determined, piece-wise constant source density functions are replaced by functions which, with their first derivatives, are continuous on the boundary. In contrast to other reported results, this modification permits one to compute unknown boundary stress components directly from the approximate stress function without recourse to such indirect techniques as extrapolation, numerical differentiation, and others. As the result, a direct comparison between the specified boundary stresses and those boundary stresses consistent with the approximate biharmonic stress function is now made possible; and thereby the usefulness of the integral equation method in plane elasticity is considerably enhanced.

INTRODUCTION

This report is a sequel to the earlier report "An Integral Equation Method in Plane Elasticity," NASA Contractor Report, NASA CR-779 written by the same authors. The preceding report presented a direct numerical method for solving the first fundamental boundary-value problem of plane elastostatics. The method involved the formulation of the biharmonic stress function in terms of two single-layer potentials, each containing an unknown source density function. Discrete values of the source density functions were obtained numerically by assuming the source density functions to be piece-wise constant around the boundary of an elastic region.

Numerical results presented in the preceding report (ref. 1) indicate that the integral equation method is extremely accurate at a distance away from the boundary of an elastic region but that, in general, the accuracy of the numerical solution decreases as the point at which computations are performed approaches the boundary. Although reasonably accurate boundary stresses were obtained in some instances by using the computational method given in (ref. 1), the results obtained from the study of problems involving an elliptical hole in an infinite elastic

region indicates that the technique used does not yield accurate boundary stresses on portions of the boundary where, from one interval to another, the change in the value of the source density is relatively large. It is apparent from these results and from other published results (refs. 2 and 3) that an improvement in the accuracy of boundary stress computations must be made if this numerical method is to be fully exploited.

There is considerable motivation for calculating stress components at the boundary directly from the approximate stress function. This has not been done in (ref. 1) or in other published results. The use of extrapolation (ref. 2) or numerical differentiation (ref. 3) of the stress function is an indirect method and the results obtained are not consistently accurate. The method of computation used in (ref. 1) is simpler than either of the above methods and fits easily into the framework of analysis; however, it "begs the question" to the extent that only the total stress is computed directly and the specified boundary tractions are used in conjunction with the computed total stress to determine values of individual stress components.

All the methods that have been used to compute boundary stresses have the same deficiency; that is, they do not permit a direct comparison between the specified boundary tractions and those that are implied by the existence of the stress function. The idea involved here is that the stress function satisfies the field equation automatically and one should be able to compute the boundary tractions with which the stress function is consistent. The comparison between the specified boundary tractions and the computed tractions provides an excellent criterion for assessing the accuracy of approximate solutions.

If directly computed boundary tractions are not available, the only means available to evaluate the validity of a solution is to establish convergence of numerical solutions. Convergence can only be assessed by solving the problem repeatedly with increasingly finer boundary subdivisions until no appreciable change in results is observed. From the results in (ref. 1), it is clear that the rate of convergence is slowest on or near the boundary and that, in many instances, the present computational capability may not be sufficient to establish convergence of a numerical solution at all points. As the simultaneous algebraic equations used to determine source density values inherently become more ill-conditioned as the number of boundary subdivisions increases, the problem of obtaining convergent solutions quickly degenerates to the various problems met in dealing with imperfect computing machinery.

The technique used to overcome these difficulties is to replace the piecewise constant source density functions with density functions which, with their first derivatives, are continuous on the boundary. These continuity conditions are required if the boundary stress components are to be defined directly in terms of the appropriate second derivatives of the approximate biharmonic stress function.

For the sake of completeness, the integral equation method presented in the preceding report (ref. 1) is briefly described in the following section. Subsequent sections present: 1) source density continuity requirements, 2) representations of the source density functions, 3) formulas for boundary stress components, and 4) the computational techniques. Finally, numerical results are presented and discussed for an exterior problem.

THE INTEGRAL EQUATION METHOD

The problem of determining the stress field in a planar region, subjected to specified boundary loadings, may be posed mathematically as one of finding a stress function χ which is related to the stress components by the equations

$$\sigma_x = \frac{\partial^2 \chi}{\partial y^2} \quad , \quad \sigma_y = \frac{\partial^2 \chi}{\partial x^2} \quad , \quad \tau_{xy} = - \frac{\partial^2 \chi}{\partial x \partial y} \quad . \quad (1)$$

The stress function will satisfy the compatibility and equilibrium equations provided it is a solution to the biharmonic equation within the region of interest; that is,

$$\nabla^2 \nabla^2 \chi(P) = 0, \quad P(x,y) \text{ in } D. \quad (2)$$

The stress components defined by (1) must be consistent with the state of stress specified on the boundary L of the domain D . If F_x and F_y are the stress components in the x and y directions specified on L , then the boundary conditions may be written, using equations (1), as

$$\left. \begin{aligned} - F_x &= \frac{dx}{dn} \frac{\partial^2 \chi}{\partial y^2} - \frac{dy}{dn} \frac{\partial^2 \chi}{\partial x \partial y} \\ - F_y &= \frac{dy}{dn} \frac{\partial^2 \chi}{\partial x^2} - \frac{dx}{dn} \frac{\partial^2 \chi}{\partial x \partial y} \end{aligned} \right\} \text{ on } L \quad (3)$$

where \bar{n} is the normal to L directed inward toward D . The notation employed is depicted in Figure 1.

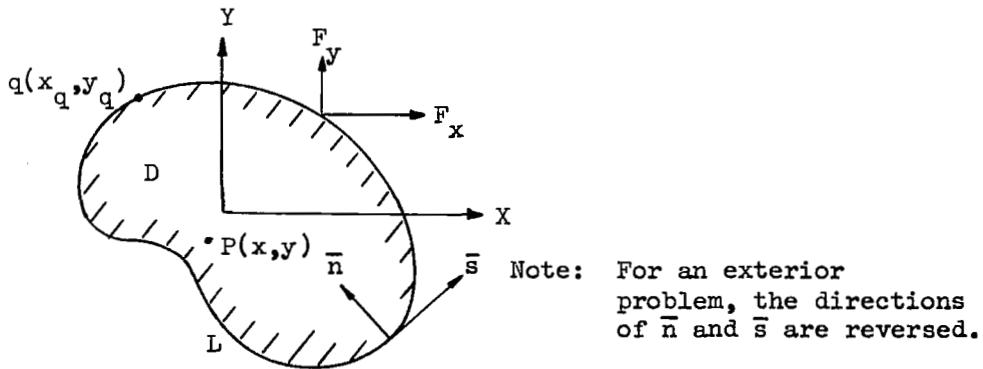


Figure 1. -Sign convention for an interior domain.

The general representation taken for the biharmonic function is

$$\chi(P) = r^2(P) \phi(P) + \psi(P) \quad (4)$$

where $r(P) = (x^2 + y^2)^{1/2}$, and both ϕ and ψ are harmonic functions;

$$\nabla^2 \phi(P) = 0, \quad \nabla^2 \psi(P) = 0; \quad P \text{ in } D.$$

The single-layer potentials

$$\phi(P) = \int_L \sigma(q) \log |P - q| dq \quad (5)$$

$$\psi(P) = \int_L \mu(q) \log |P - q| dq \quad (6)$$

are both harmonic within D , as σ and μ are defined only on L and $\log |P - q|$ is harmonic. Integration is over the entire boundary and dq is a scalar element of arc on L . Substitution of (5) and (6) into (4) yields

$$\chi(P) = r^2(P) \int_L \sigma(q) \log |P - q| dq + \int_L \mu(q) \log |P - q| dq \quad (7)$$

which is a biharmonic function involving two unknown functions σ and μ , commonly termed source density functions.

The representation given by (7) is complete only for a simply-connected interior domain. If an exterior domain is under consideration, then, in order to insure single-valued displacements, it is necessary to require that $\int_L \sigma(q) dq = 0$ and a constant must be added to the representation given by (7) to insure completeness.

Equations (3) may be used to derive the canonical boundary conditions:

$$\chi(s) = - \int_{s_0}^s \frac{dx}{ds} \left[\int_{s_0}^s F_y ds \right] ds + \int_{s_0}^s \frac{dy}{ds} \left[\int_{s_0}^s F_x ds \right] ds + \alpha x + \beta y + \gamma \quad (8)$$

and

$$\frac{d\chi(s)}{dn} = - \frac{dx}{dn} \int_{s_0}^s F_y ds + \frac{dy}{dn} \int_{s_0}^s F_x ds + \alpha \frac{dx}{dn} + \beta \frac{dy}{dn}, \quad (9)$$

where s is measured along the boundary L ; s_0 designates an arbitrary point on L ; and α , β , and γ are constants of integration which may be set to zero for problems involving either interior or exterior domains. Note that equations (8) and (9) permit χ and $\frac{d\chi}{dn}$ to be computed directly once the boundary tractions and the boundary geometry are specified.

The boundary-value problem originally defined by (2) and (3) is now presented in canonical form by (2), (8) and (9). Since the representation of χ provided by (7) automatically satisfies (2), the boundary-value problem is solved formally by requiring (7) to satisfy (8) and (9). These two boundary equations lead to two coupled integral equations for the determination of $\sigma(q)$ and $\mu(q)$. It is generally impossible to solve the coupled integral equations exactly; therefore, a numerical method is used to obtain approximate solutions.

The numerical solution is accomplished by subdividing the boundary L into m subdivisions numbered in the direction of increasing s . Within each interval the $\sigma(q)$ and $\mu(q)$ are assigned unknown constant values σ_i and μ_i ; $i = 1, 2, \dots, m$. The length of the i -th interval is denoted by h_i . Because the source densities are assumed to be piece-wise constant, the integral equations become simultaneous algebraic equations if one requires the boundary conditions (8) and (9) to be satisfied at each interval center point p_j ; $j = 1, 2, \dots, m$. These equations may be solved for the unknowns σ_i and μ_i ; $i = 1, 2, \dots, m$. For the work presented in (ref. 1), the numerical solution took the following form

$$\chi(P) = r^2(P) \sum_{i=1}^m \sigma_i \int_i \log|P - q|dq + \sum_{i=1}^m \mu_i \int_i \log|P - q|dq \quad (10)$$

where \int_i indicates integration over the i -th interval.

With this background concerning the basis of the integral equation method, let us proceed to consider the modifications implemented to improve the accuracy of the approximate solution and to permit the direct computation of boundary stresses.

CONSIDERATION OF SOURCE DENSITY CONTINUITY

In order to compute boundary stresses directly from the approximate stress function, it is necessary to impose certain continuity conditions on the approximate source density functions. These conditions are suggested by the following discussion.

Consider a portion of the boundary L to be a line segment of length h and the boundary point p under consideration to be at a midpoint of this segment. As shown in Figure 2, locate a coordinate system with origin at p with axes η and ϵ respectively tangent and perpendicular to the line segment.

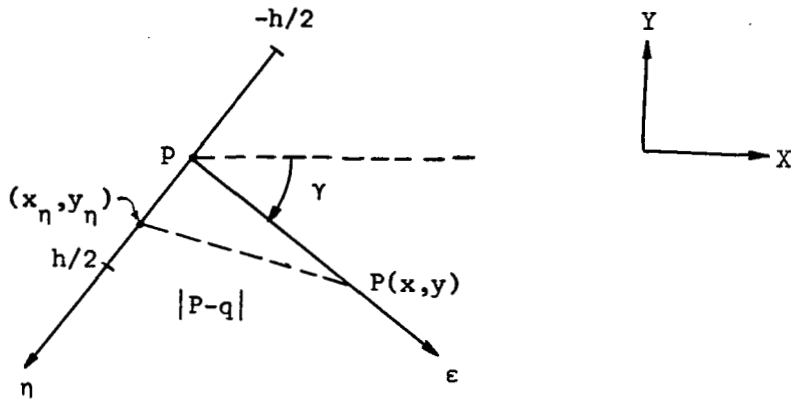


Figure 2. -Notation used in considering source density continuity.

The limiting values of the second derivatives of the potential

$$I = \int_h \rho(q) \log |P - q| dq \quad (11)$$

will be derived as the field point P located as shown in Figure 2 approaches p along the line $\eta = 0$ (\int_h represents integration over the line segment). For this example, the source density function ρ is represented by

$$\rho^1(\eta) = \rho_1 + t_1\eta + v_1\eta^2, \quad 0 < \eta \leq h/2 \quad (12)$$

$$\rho^2(\eta) = \rho_2 + t_2\eta + v_2\eta^2, \quad -h/2 \leq \eta < 0. \quad (13)$$

The limits to be evaluated are

$$\bar{I}_{xx} = \lim_{\substack{\epsilon \rightarrow 0 \\ \eta=0}} \frac{\partial^2 I}{\partial x^2} \quad (14)$$

and

$$\bar{I}_{xy} = \lim_{\substack{\epsilon \rightarrow 0 \\ \eta=0}} \frac{\partial^2 I}{\partial x \partial y} \quad (15)$$

Note that $\nabla^2 I = 0$ so that $\frac{\partial^2 I}{\partial x^2} = -\frac{\partial^2 I}{\partial y^2}$ and, therefore, $\bar{I}_{yy} = -\bar{I}_{xx}$, provided the limit indicated in (14) exists. Using (x_η, y_η) to denote a point q on the line segment, it follows from (11) that

$$\frac{\partial^2 I}{\partial x^2} = 2 \int_h \frac{\rho(\eta)[(y - y_\eta)^2 - (x - x_\eta)^2] d\eta}{|P - q|^4} \quad (16)$$

and

$$\frac{\partial^2 I}{\partial x \partial y} = -2 \int_h \frac{\rho(\eta)(y - y_\eta)(x - x_\eta) d\eta}{|P - q|^4}, \quad (17)$$

where

$$|P - q|^4 = [(x - x_\eta)^2 + (y - y_\eta)^2]^2.$$

Since P is located on the line $\eta = 0$, it is clear that

$$x - x_\eta = \epsilon \cos \gamma + \eta \sin \gamma,$$

$$y - y_\eta = -\epsilon \sin \gamma + \eta \cos \gamma,$$

$$|P - q|^4 = (\epsilon^2 + \eta^2)^2,$$

where γ is the angular coordinate as shown in Figure 2.

The integrals obtained by substituting the above relations, equations (12) and (13) into (16) and (17) can be evaluated analytically. When $\epsilon \ll h/2$, equations (16) and (17) can be reduced to as follows:

$$\begin{aligned} \frac{\partial^2 I}{\partial x^2} &\rightarrow \frac{-2}{h} (\rho_1 + \rho_2) \cos 2\gamma - (t_2 - t_1) \cos 2\gamma \log \epsilon \\ &+ \frac{(\rho_2 - \rho_1) \sin 2\gamma}{\epsilon} - \frac{\pi}{2} (t_1 + t_2) \sin 2\gamma \\ &+ \frac{h}{2} (v_1 + v_2) \cos 2\gamma \end{aligned}$$

$$\begin{aligned} \frac{\partial^2 I}{\partial x \partial y} \rightarrow & \frac{2}{h} (\rho_1 + \rho_2) \sin 2\gamma + (t_2 - t_1) \sin 2\gamma \log \epsilon \\ & - \frac{\pi}{2} (t_1 + t_2) \cos 2\gamma + \frac{(\rho_2 - \rho_1) \cos 2\gamma}{\epsilon} \\ & + \frac{h}{2} (v_1 + v_2) \sin 2\gamma . \end{aligned}$$

From the above expressions it can be seen that the limits \bar{I}_{xx} and \bar{I}_{xy} given by equations (14) and (15) exist only when $\rho_1 = \rho_2$ and $t_2 = t_1$. From equations (12) and (13), it is evident that these conditions are equivalent to requiring that $\rho(\eta)$ and its first derivative be continuous at p . Note that no restrictions are imposed on the coefficients v_1 and v_2 so that a bounded discontinuity in the second derivative of a source density function is permissible. It is evident from the above discussion that the representation of the source densities as piece-wise constant functions automatically precludes the possibility of computing boundary stresses directly from an approximate stress function having the form given by equation (10).

REPRESENTATION OF THE SOURCE DENSITY FUNCTIONS

Within each of the m boundary subdivisions of the boundary L , the source density functions are represented in terms of the coordinate s measured in the direction of \bar{s} as follows:

$$\sigma^i(s) = \sigma_i + t_{\sigma i} v + v_{\sigma i} v^2; \quad i = 1, 2, \dots, m \quad (18 a)$$

$$\mu^i(s) = \mu_i + t_{\mu i} v + v_{\mu i} v^2; \quad i = 1, 2, \dots, m \quad (18 b)$$

where $v = (s - s_i)/h_i$ ($0 \leq v \leq 1$) and s_i is the value of s at the beginning of the i^{th} interval.

One must require continuity of the source densities and their derivatives at each interval end-point. Hence, if $\rho^i(s) = \rho_i + t_i v + v_i v^2$ represents either $\sigma^i(s)$ or $\mu^i(s)$; $i = 1, 2, \dots, m$, it is necessary that

$$\rho^i(s_{i+1}) = \rho^{i+1}(s_{i+1}) ,$$

$$\frac{d\rho^i(s_{i+1})}{ds} = \frac{d\rho^{i+1}(s_{i+1})}{ds} .$$

These two equations yield the relations

$$\rho_i + t_i + v_i = \rho_{i+1}; \quad i = 1, 2, \dots, m-1 \quad (19 a)$$

and

$$\frac{t_i + 2v_i}{h_i} = \frac{t_{i+1}}{h_{i+1}}; \quad i = 1, 2, \dots, m-1, \quad (19 b)$$

while for the case when $i = m$ one has

$$\rho_m + t_m + v_m = \rho_1 \quad (19 c)$$

and

$$(t_m + 2v_m)/h_m = t_1/h_1. \quad (19 d)$$

In the case of an exterior problem, it is necessary to insure that

$$\int_L \sigma(s) ds = 0.$$

In terms of the representation given above, this constraint is equivalent to

$$\sum_{i=1}^m h(\sigma_i + \frac{1}{2} t_{\sigma i} + \frac{1}{3} v_{\sigma i}) = 0. \quad (20)$$

In order to completely specify a source density function using (18), it is necessary to determine the $3m$ coefficients ρ_i , t_i , and v_i ; $i = 1, 2, \dots, m$, subject to the $2m$ constraints given by (19). Therefore, if one value of a source density is known within each boundary subdivision, it is possible to form equations in the $3m$ unknowns whose solutions completely specify a source density function in terms of the assumed representation (18). In the case of an exterior problem, the system of equations becomes overdetermined because equation (20) provides another constraint. Of course, the known value of σ within each interval should have been determined in accordance with a constraint analogous to (20) so that this constraint will always be nearly satisfied by the solutions to the $3m$ equations. It is a simple matter then to make a slight adjustment to the values of the σ_i which insures that (20) is satisfied.

If the problem under consideration has symmetry with respect to both the x and y axes, then the number of coefficients which must be determined to specify each source density function is only $3m/4$. In this instance the system governing the unknown coefficients is overdetermined in any circumstance because, in order

to preserve the symmetry, it is necessary to require that the derivative of each source density be zero at the points where the boundary intersects the x and y axes. That is, if $k = m/4$, then t_1, t_{k+1}, t_{2k+1} , and t_{3k+1} must be zero when ρ represents either σ or μ . This overdeterminacy presents no real problem, however, and in fact, can be used to simplify the determination of the unknown coefficients. Suppose that the value of each source density is known at the interval end point; that is, the ρ_i are specified. Then, using the fact that t_1 is equal to zero, we can determine v_1 from the first of the equations (19) by considering the case $i = 1$. Then t_2 can be determined from the second equation and the whole process can be repeated for $i = 2, 3, \dots, m$. In this way all the required coefficients can be determined without having to solve a large set of simultaneous equations.

Prior to determining these unknown coefficients in this manner, conditioning of the known ρ_i must be performed in order to insure that t_{k+1} is equal to zero. Let $\rho_i, i = 1, 2, \dots, m+1$, be the known values of a source density at the interval end points. Let ρ_i^* be those values of the source density which insure that t_{k+1} is equal to zero. It can be shown that

$$t_{k+1} = 2(-1)^k \sum_{i=1}^k (-1)^i (\rho_{i+1} - \rho_i),$$

hence, one obtains

$$0 = 2(-1)^k \sum_{i=1}^k (-1)^i (\rho_{i+1}^* - \rho_i^*).$$

This condition will be satisfied provided we compute the ρ_i^* from the equation

$$\rho_i^* = \rho_i + \alpha(-1)^i$$

where

$$\alpha = \frac{1}{2k} \sum_{j=1}^k (-1)^j (\rho_{j+1} - \rho_j).$$

Note that as the number of boundary intervals is increased, the difference between ρ_i^* and the ρ_i will decrease. For the numerical examples considered, the parameter α is quite small and this conditioning process has little effect on the accuracy of the specified source densities.

The final step in the conditioning process is performed after the constants t_i and $v_i, i = 1, 2, \dots, k$, have been determined. To insure that $\int_L \sigma(s) ds = 0$,

one computes the quantity

$$A = \sum_{i=1}^k h_i (\sigma_i^* + \frac{1}{2} t_{\sigma_i} + \frac{1}{3} v_{\sigma_i}) ,$$

and

$$\sigma_i^{**} = \sigma_i^* - \frac{A}{\sum_{j=1}^k h_j} .$$

If the numbers σ_i^{**} are used in the representation of $\sigma(s)$, all necessary conditions will be satisfied by the representations of the source density functions. Note that the σ_i^{**} , $i = 1, 2, \dots, k+1$, still satisfy the equation

$$0 = 2(-1)^k \sum_{i=1}^k (-1)^i (\sigma_{i+1}^{**} - \sigma_i^{**})$$

as the difference between σ_i^{**} and σ_i^* is a constant for all i . In the work that follows it can be assumed that source density coefficients have been conditioned properly. Asterisks will no longer be used to indicate proper conditioning.

REPRESENTATIONS FOR BOUNDARY STRESSES

In order to completely specify the state of stress at a given point $p(x,y)$ on L , the total stress and the normal and shear stress tangent to the boundary will be calculated. The total stress, θ , is simply $\nabla^2 \chi$. To develop formulas for the shear and normal stresses, define a rectangular coordinate system with origin at $p(x,y)$ and the axes η and ϵ measured in the direction of \bar{s} and \bar{n} respectively. Then the tangential stress, σ_t , is defined in terms of the stress function by the equation

$$\sigma_t = \lim_{\substack{\epsilon \rightarrow 0 \\ \eta = 0}} \frac{\partial^2 \chi(P)}{\partial \epsilon^2} \quad (21)$$

and the shear stress, τ_t , is given by

$$\tau_t = -\lim_{\substack{\epsilon \rightarrow 0 \\ \eta = 0}} \frac{\partial^2 \chi(P)}{\partial \epsilon \partial \eta} \quad (22)$$

Therefore, in order to calculate the boundary stresses directly from equation (7), one must evaluate expressions of the following type.

$$I^{\rho} = \lim_{\substack{\epsilon \rightarrow 0 \\ \eta = 0}} S_{\rho} , \quad I_{\epsilon}^{\rho} = \lim_{\substack{\epsilon \rightarrow 0 \\ \eta = 0}} \frac{\partial S_{\rho}}{\partial \epsilon} , \quad (23 \text{ a,b})$$

$$I_{\eta}^{\rho} = \lim_{\substack{\epsilon \rightarrow 0 \\ \eta = 0}} \frac{\partial S_{\rho}}{\partial \eta} , \quad I_{\epsilon\epsilon}^{\rho} = \lim_{\substack{\epsilon \rightarrow 0 \\ \eta = 0}} \frac{\partial^2 S_{\rho}}{\partial \epsilon^2} , \quad (23 \text{ c,d})$$

and

$$I_{\eta\epsilon}^{\rho} = \lim_{\substack{\epsilon \rightarrow 0 \\ \eta = 0}} \frac{\partial^2 S_{\rho}}{\partial \epsilon \partial \eta} , \quad (23 \text{ e})$$

where

$$S_{\rho} = \int_L \rho(q) \log |P-q| dq \quad (24)$$

and we have used ρ to represent either σ or μ .

The formulas at $p(x,y)$ for the total stress and the shear and normal stresses parallel to the boundary can be written in terms of the above expressions as:

$$\theta(p) = 4I^{\sigma} + 2\left[\frac{\partial r^2}{\partial \epsilon} I_{\epsilon}^{\sigma} + \frac{\partial r^2}{\partial \eta} I_{\eta}^{\sigma}\right] , \quad (25 \text{ a})$$

$$\sigma_t(p) = r^2 I_{\epsilon\epsilon}^{\sigma} + 2\frac{\partial r^2}{\partial \epsilon} I_{\epsilon}^{\sigma} + \frac{\partial^2 r^2}{\partial \epsilon^2} I^{\sigma} + I_{\epsilon\epsilon}^{\mu} , \quad (25 \text{ b})$$

$$\tau_t(p) = -r^2 I_{\eta\epsilon}^{\sigma} - \frac{\partial r^2}{\partial \eta} I_{\epsilon}^{\sigma} - \frac{\partial r^2}{\partial \epsilon} I_{\eta}^{\sigma} - \frac{\partial^2 r^2}{\partial \epsilon \partial \eta} I^{\sigma} - I_{\eta\epsilon}^{\mu} . \quad (25 \text{ c})$$

Equations (25 a-c) give representations for the boundary stress components, and the next section deals with the evaluation of the limits appearing in these equations.

BOUNDARY APPROXIMATIONS AND LIMIT FORMULAS

Though, ideally, one would like to have formulas which permit the calculation of boundary stresses using equations (25) at any point $p(x,y)$ on the boundary, the following discussion will be restricted to the evaluation of the required limit when the point under consideration is an interval end point. There is no special reason for such a restriction; that is, it is possible to use equations (25) wherever boundary continuity conditions are met. However, the development of a

computational scheme to handle any boundary point would be fraught with notational difficulties. It is simpler to perform the partitioning of the boundary so that the selected computational points correspond to interval end points. With this understanding, let us proceed to develop formulas for the evaluation of equations (25) at interval end points.

Assume the point $p(x,y)$ to be at the beginning of interval $i+1$ (at $s = s_{i+1}$). It is clear that except in the intervals i and $i+1$ the integrands of the potential functions and their derivatives are well-behaved. Therefore, one may consider each of the integrals in equations (23) to be the sum of two integrals. One integral extends over the i and $i+1$ intervals while the other extends over the remainder of the boundary. For integrals of the latter type, the required limits may be formed by simply replacing P by p in the integrals. The resulting integrals may be evaluated accurately using Simpson's rule.

In evaluating the limits of integrals over intervals i and $i+1$, it is necessary to perform the required integration and differentiation and to substitute zero for η prior to taking the indicated limit.

The fundamental approximation made in evaluating the integrals over the i and the $i+1$ intervals is to replace the boundary segments within each of these intervals by circular arcs tangent at the point p . Associated with each of these arcs are radii R_i and R_{i+1} and included angles δ_i and δ_{i+1} respectively. Angular coordinates α and $\bar{\alpha}$ as well as other notations are illustrated in Figure 3.*

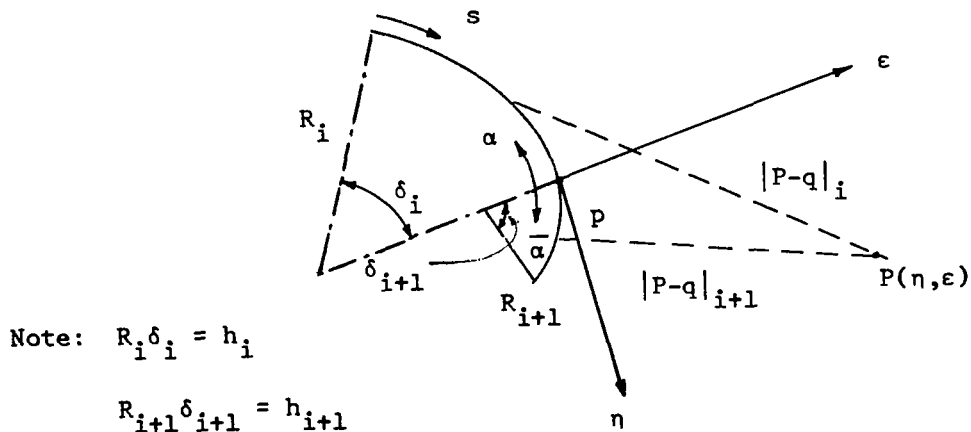


Figure 3. -Boundary approximation used to evaluate limits.

*The formulas derived from the geometry shown in Figure 3 do not cover all possible situations, since in this figure, the coordinate ϵ is directed away from the centers of both arcs. In the general case, the coordinate ϵ may be directed toward or away from the center of either arc depending on the shape of the boundary.

From the geometry illustrated in Figure 3 it can be shown that

$$|P-q|_i^2 = (2R_i^2 + 2\epsilon R_i) (1-\cos \alpha) + 2R_i \eta \sin \alpha + \epsilon^2 + \eta^2$$

for $0 \leq \alpha \leq \delta_i$, and that

$$|P-q|_{i+1}^2 = (2R_{i+1}^2 + 2\epsilon R_{i+1})(1-\cos \bar{\alpha}) - 2R_{i+1} \eta \sin \bar{\alpha} + \epsilon^2 + \eta^2$$

for $0 \leq \bar{\alpha} \leq \delta_{i+1}$.

In terms of the parameters α and $\bar{\alpha}$, the representations of the source densities $\rho^i(s)$ and $\rho^{i+1}(s)$ become respectively,

$$\rho^i(\alpha) = \rho_{i+1} - \frac{\alpha}{\delta_i}(t_i + 2v_i) + \frac{\alpha^2 v_i}{\delta_i^2} \quad (26)$$

$$\rho^{i+1}(\bar{\alpha}) = \rho_{i+1} + \frac{\bar{\alpha}}{\delta_{i+1}} t_{i+1} + \frac{\bar{\alpha}^2 v_{i+1}}{\delta_{i+1}^2} \quad (27)$$

The continuity conditions imposed on $\rho(s)$ can be written as *

$$\rho_i + t_i + v_i = \rho_{i+1} \quad (28)$$

$$\frac{t_i + 2v_i}{R_i \delta_i} = \frac{t_{i+1}}{R_{i+1} \delta_{i+1}} \quad (29)$$

If \bar{S}_ρ is the contribution to S_ρ , equation (24), from integration over intervals i and $i+1$, then one has

*The notation $\rho(s)$ is used as before to signify either $\sigma(s)$ or $\mu(s)$.

$$\begin{aligned}
\bar{S}_\rho = & \frac{R_i}{2} \int_0^{\delta_i} \rho^i(\alpha) \log[(2R_i^2 + 2\epsilon R_i)(1 - \cos \alpha) + 2R_i \eta \sin \alpha + \epsilon^2 + \eta^2] d\alpha \\
& + \frac{R_{i+1}}{2} \int_0^{\delta_{i+1}} \rho^{i+1}(\bar{\alpha}) \log[(2R_{i+1}^2 + 2\epsilon R_{i+1})(1 - \cos \bar{\alpha}) \\
& - 2R_{i+1} \eta \sin \bar{\alpha} + \epsilon^2 + \eta^2] d\bar{\alpha} .
\end{aligned} \tag{30}$$

If H^ρ , H_ϵ^ρ , H_η^ρ , $H_{\epsilon\epsilon}^\rho$, and $H_{\eta\epsilon}^\rho$ are the limits given by equations (23) when \bar{S}_ρ is substituted for S_ρ , then, using equations (26) through (30), the following results can be obtained.*

$$\begin{aligned}
H^\rho = & \frac{R_i}{2} \int_0^{\delta_i} \rho^i(\alpha) \log[2R_i^2(1 - \cos \alpha)] d\alpha \\
& + \frac{R_{i+1}}{2} \int_0^{\delta_{i+1}} \rho^{i+1}(\alpha) \log[2R_{i+1}^2(1 - \cos \alpha)] d\alpha
\end{aligned} \tag{31 a}$$

$$\begin{aligned}
H_\epsilon^\rho = & \rho_{i+1} \left(\pi + \frac{1}{2}(\delta_i + \delta_{i+1}) \right) - \frac{(t_i + 2v_i)}{4} \delta_i + \frac{v_i \delta_i}{6} \\
& + \frac{t_{i+1}}{4} \delta_{i+1} + \frac{v_{i+1}}{6} \delta_{i+1}
\end{aligned} \tag{31 b}$$

$$\begin{aligned}
H_\eta^\rho = & \frac{1}{2\rho_{i+1}} \log \frac{(1 - \cos \delta_i)}{(1 - \cos \delta_{i+1})} + \frac{1}{2\delta_i^2} \int_0^{\delta_i} \frac{[v_i \alpha^2 - \alpha \delta_i (t_i + 2v_i)] \sin \alpha d\alpha}{1 - \cos \alpha} \\
& - \frac{1}{2\delta_{i+1}^2} \int_0^{\delta_{i+1}} \frac{[\alpha t_{i+1} \delta_{i+1} + \alpha^2 v_{i+1}] \sin \alpha d\alpha}{1 - \cos \alpha}
\end{aligned} \tag{31 c}$$

*The derivation of these results is outlined in Appendix A.

$$\begin{aligned}
H_{\epsilon\epsilon}^{\rho} = & -\frac{\rho_{i+1}}{2} \left\{ \frac{\delta_i + \pi}{R_i} + \frac{\text{ctn}(\frac{1}{2}\delta_i)}{R_i} + \frac{\delta_{i+1} + \pi}{R_{i+1}} + \frac{\text{ctn}(\frac{1}{2}\delta_{i+1})}{R_{i+1}} \right\} \\
& + \frac{t_{i+1}}{2R_{i+1}\delta_{i+1}} \int_{\delta_i}^{\delta_{i+1}} \frac{\alpha \cos \alpha d\alpha}{1-\cos \alpha} + \frac{v_i}{2\delta_i^2 R_i} \int_0^{\delta_i} \frac{\alpha^2 \cos \alpha d\alpha}{1-\cos \alpha} \\
& + \frac{v_{i+1}}{2R_{i+1}\delta_{i+1}^2} \int_0^{\delta_{i+1}} \frac{\alpha^2 \cos \alpha d\alpha}{1-\cos \alpha}, \tag{31 d}
\end{aligned}$$

$$\begin{aligned}
H_{\eta\epsilon}^{\rho} = & \frac{\rho_{i+1}}{r_i} \log\left(\frac{1-\cos\frac{h_{i+1}}{r_i}}{1-\cos\frac{h_i}{r_i}}\right) + \frac{\pi t_{i+1}}{R_{i+1}\delta_{i+1}} \\
& + \frac{t_{i+1}}{2R_{i+1}\delta_{i+1}} \left\{ \int_0^{\delta_i} \frac{\alpha \sin \alpha d\alpha}{1-\cos \alpha} + \int_0^{\delta_{i+1}} \frac{\alpha \sin \alpha d\alpha}{1-\cos \alpha} \right\} \\
& + \frac{v_{i+1}}{2R_{i+1}\delta_{i+1}^2} \int_0^{\delta_{i+1}} \frac{\alpha^2 \sin \alpha d\alpha}{1-\cos \alpha} - \frac{v_i}{2R_i\delta_i^2} \int_0^{\delta_i} \frac{\alpha^2 \sin \alpha d\alpha}{1-\cos \alpha}, \tag{31 e}
\end{aligned}$$

where $r_i = (R_i + R_{i+1})/2$. The variable α appears only as a variable of integration in equations (31) so that there is no reason to distinguish between α and $\bar{\alpha}$.

Some comments are in order with regard to equations (31). First some expressions are left in terms of integrals for the sake of conciseness. The first integral appearing in equation (31 d) can be written as

$$\begin{aligned}
\int_{\delta_i}^{\delta_{i+1}} \frac{\alpha \cos \alpha d\alpha}{1-\cos \alpha} = & \frac{\delta_i^2 - \delta_{i+1}^2}{2} + 2 \log \left(\frac{\sin \frac{1}{2}\delta_{i+1}}{\sin \frac{1}{2}\delta_i} \right) \\
& - \delta_{i+1} \text{ctn} \frac{1}{2}\delta_{i+1} + \delta_i \text{ctn} \frac{1}{2}\delta_i.
\end{aligned}$$

The last two integrals in equation (31 d) can be evaluated from the formula:

$$\int_0^{\delta} \frac{\alpha^2 \cos \alpha d\alpha}{1-\cos \alpha} = \frac{-\delta^3}{3} - \delta^2 \text{ctn} \frac{1}{2}\delta + 4\delta \sum_{j=0}^{\infty} \frac{(-1)^j B_{2j} \delta^{2j}}{(2j+1)(2j)!}$$

where $\{B_{2j}; j = 0, 1, 2, \dots\}$ are the Bernoulli numbers. All remaining integrals

may be reduced to the following type:

$$I^k(\delta) = \int_0^\delta \alpha^k \log(1-\cos \alpha) d\alpha = \frac{\delta^k}{k+1} \left[\log(1-\cos \delta) - 2 \sum_{j=0}^{\infty} \frac{(-1)^j B_{2j} \delta^{2j}}{(2j+k+1)(2j)!} \right];$$

$$k = 0, 1, 2, \dots$$

as

$$\int_0^\delta \frac{\alpha^k \sin \alpha d\alpha}{1-\cos \alpha} = \delta^k \log(1-\cos \delta) - k \int_0^\delta \alpha^{k-1} \log(1-\cos \alpha) d\alpha.$$

It should be noted that the first term on the right-hand side of equation (31 e) cannot be derived if the boundary is approximated as shown in Figure 3. The tangent circular arcs create a boundary with a discontinuity in the curvature at p.

This discontinuity causes the expression $\lim_{\epsilon \rightarrow 0} \frac{\partial \bar{S}}{\partial \epsilon \partial \eta}$ to have a logarithmic singularity in the term with coefficient ρ_{i+1} .

The term given in equation (31 e) is an adequate approximation to the results obtained from more detailed analysis which establishes the existence of the limit provided there is no discontinuity in the curvature of the boundary.

The relations given by equations (31 a) through (31 c) are simply special presentations of well-known results in potential theory. The results given in equations (31 d) and (31 e) have not been found in any publications. It is emphasized that the limits represented by these equations do not exist, no matter what boundary geometry is assumed, unless the source densities and their first derivatives with respect to the variable s are continuous on L.

THE NUMERICAL CALCULATION OF BOUNDARY STRESSES

The results given in the preceding chapters permit the development of a computational scheme to calculate the boundary stresses at interval end points using equations (25). The computational method developed will be outlined in this section.

$$\text{Evaluation of } I^0, I_\epsilon^0, I_\eta^0, I_{\epsilon\epsilon}^0, \text{ and } I_{\eta\epsilon}^0$$

As discussed in the preceding section, each of the limits appearing in equations (25) is considered as the sum of two parts. If the selected boundary point is at s_{i+1} (the beginning of interval $i+1$), then one part is the limit of the integration over intervals i and $i+1$ while the other part is the limit of the integration over the remainder of the boundary. The former limits can be evaluated using the formulas for $H^0, H_\epsilon^0, H_\eta^0, H_{\epsilon\epsilon}^0, \text{ and } H_{\eta\epsilon}^0$ given by equations (31).

The integration formulas given in the discussion following these equations can be used to evaluate the required integrals.

The limits of integrals over the boundary complement of intervals i and $i+1$ are evaluated using Simpson's rule. For $j = 1, 2, \dots, m$; $j \neq i-1, i, i+1, \text{ or } i+2$; integrands are evaluated at interval end and center points for substitution into Simpson's rule. That is, if

$$F(p) = \int_j f(p,q) dq; \quad j \neq i-1, i, i+1, i+2$$

represents the integral to be evaluated, one uses

$$F(p) \approx \frac{h_j}{6} [f(p, q_{j-\frac{1}{2}}) + 4f(p, q_j) + f(p, q_{j+\frac{1}{2}})]. \quad (32)$$

In practice, instead of using Simpson's rule to evaluate the first and second derivatives of integrals of this type with respect to the variables ϵ and η , Simpson's rule is used to calculate the required derivatives with respect to x and y . Then the chain rule for differentiation is used to determine the required derivatives with respect to ϵ and η .

Integration Over Intervals $i-1$ and $i+2$

The reason for not using equation (32) to evaluate integrals over intervals $i-1$ and $i+2$ is indicated by Figure 10 in (ref. 1). The curves shown in this figure illustrate that if the ratio of the minimum distance from the interval to the length of the interval is less than 1.25, an integration error of greater than one percent can occur if only interval end and center points are used in Simpson's rule. Therefore, within intervals $i-1$ and $i+2$, integrands are evaluated at several boundary points to maintain integration accuracy. Note that if the boundary is divided into intervals of greatly different lengths, then equation (32) may not be sufficiently accurate even when the point $p(x,y)$ is approximately two interval lengths away from the interval of integration.

The method used to evaluate integrals is illustrated below for interval $i+2$. As shown in Figure 4, this interval is approximated by a circular arc with radius R_{i+2} and an included angle of δ_{i+2} . The center of this arc is located at (x_r, y_r) with respect to the x - y axes. A coordinate system with axes \bar{x} and \bar{y} is located as shown in Figure 4.

If (\bar{x}_s, \bar{y}_s) is the location of a variable point on the interval $i+2$ relative to axes \bar{x} and \bar{y} , then using the notation shown in Figure 4, one can write

$$\bar{x}_s = d \cos(\omega+\gamma), \quad \bar{y}_s = d \sin(\omega+\gamma)$$

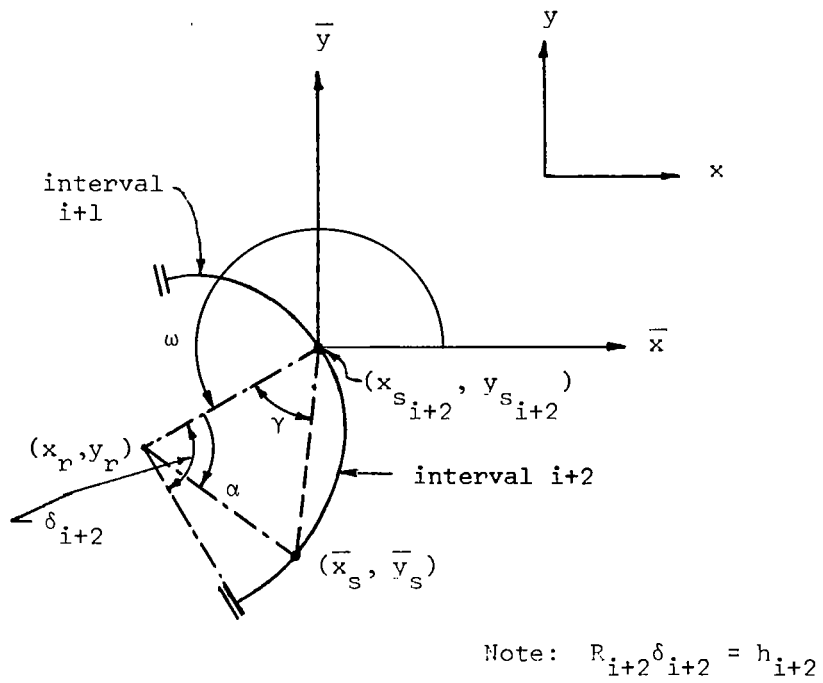


Figure 4. -Description of Interval i+2.

where

$$\gamma = \frac{1}{2}(\pi - \alpha), \quad d = 2R_{i+2} \sin \gamma/2$$

$$\omega = \tan^{-1} \left(\frac{\bar{y}_s}{\bar{x}_s} \right), \quad \bar{x}_r = x_r - x_{s_{i+2}}$$

and

$$\bar{y}_r = y_r - y_{s_{i+2}}.$$

Since

$$\bar{x}_s = x_s - x_{s_{i+2}}, \quad \bar{y}_s = y_s - y_{s_{i+2}},$$

one has

$$|p-q|_{i+2}^2 = (x - \bar{x}_s - x_{s_{i+2}})^2 + (y - \bar{y}_s - y_{s_{i+2}})^2. \quad (33)$$

All integrals of the potential function and its derivatives can be formed using equation (33) over interval $i+2$. The quantities \bar{x}_s , \bar{y}_s , $\sigma^{i+2}(s)$, and $\mu^{i+2}(s)$ are expressed in terms of the angle α so that all integrands can be evaluated at incremented values of α . These results are used in Simpson's rule to compute all required integrals as accurately as necessary.

Summary of the Computational Technique

Equations (25) provide general formulas from which boundary stresses can be determined. The limits appearing in these formulas can be evaluated at interval end points using the formulas (31) and the methods just discussed.

To use the computational formulas it is necessary to represent the source density functions as described in one of the preceding sections called Representation of the Source Density Functions. The contents of that section also indicate how the coefficients used in the representations may be evaluated if values of source densities are known at one point within each boundary interval. The source density functions derived using the indicated methods are not exact and, in fact, for the same known source density values more than one set of coefficients σ_i , $t_{\sigma i}$, $v_{\sigma i}$, μ_i , $t_{\mu i}$, and $v_{\mu i}$, $i = 1, 2, \dots, m$, can be derived. Further, if the known values of the source densities are obtained through a numerical method, then there is some inaccuracy in these values. Therefore, the accuracy of the source

density representations can be determined only by comparing the specified boundary tractions with those calculated from the computed boundary stresses. In general, it is necessary to make a series of adjustments in the coefficients of v in equations (18 a) and (18 b) in order to obtain the required accuracy in the approximate stress function.

The boundary data required to compute boundary stresses includes the information necessary to perform the computations reported in (ref. 1) and also the information needed to approximate the boundary intervals by circular arcs. The method used to develop these boundary approximations is to compute the radius of curvature at the end and center points of each interval and to subsequently assign the boundary arc a radius equal to the average of these three values. The included angle for each arc is the ratio of the interval length to the average radius. The location of the center of the arc can be found using the coordinates of the interval end points and the values of the radius and the included angle.

NUMERICAL EXAMPLES

The example problem chosen to test the described method for calculating boundary stresses is that of the elliptic hole in an infinite plate subjected to internal pressure. This problem was discussed as Example 2 in (ref. 1) and relevant notation is described therein. This problem is chosen as an example for the following reasons:

- 1) Changes in the boundary contours can be accomplished by changing the axis ratio.
- 2) From results given in Figure 14 of (Ref. 1), it can be seen that changes in boundary geometry have a significant effect on the behavior of the source density functions.
- 3) The presence of a stress concentration gives the problem practical relevance because in such situations the accurate prediction of boundary stresses is of critical importance.

Discussion of Results for the Ellipse With $a/b = 2$

The computation of boundary stresses was first attempted for the problem with $a/b = 2$. Each quadrant of the elliptical boundary was divided into 32 subdivisions of equal length, denoted by h . Finally, the coefficients necessary to specify the source density functions within each boundary interval were determined. The assignment of known values of the source densities at each interval end point was accomplished using results obtained from the numerical solution to the biharmonic equation. Figure 5 presents analytical values of the tangential and shear stresses, σ_t and τ_t respectively, in terms of the parameter $4s/|L|$ where $s = 0$ is at $y = b$, $x = 0$ and $|L|$ is circumference of the ellipse. Note that for this problem the specified value of τ_t on the boundary is zero.

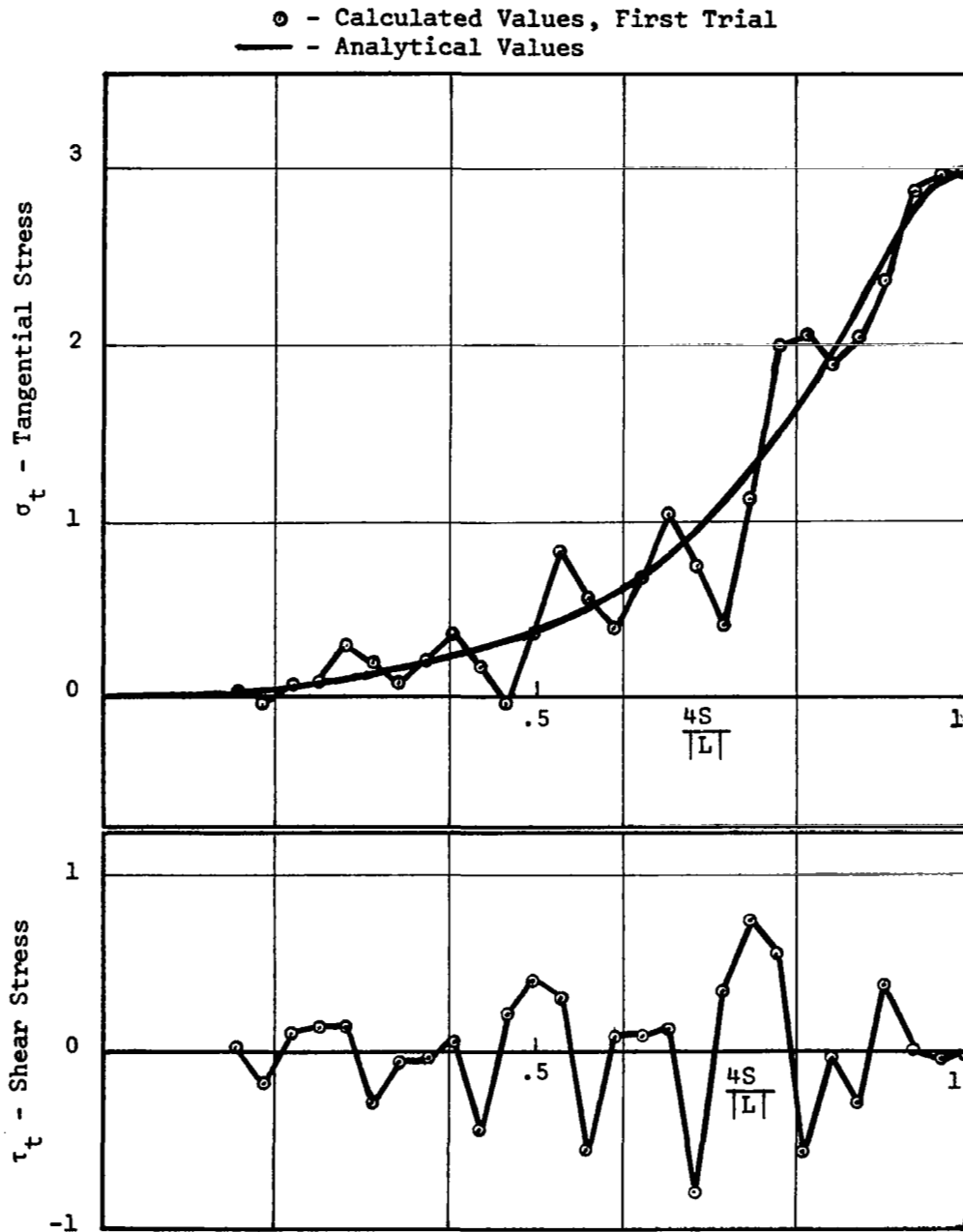


Figure 5. -Normal stress and shear stress tangent to the elliptic boundary, first trial, $a/b = 2$.

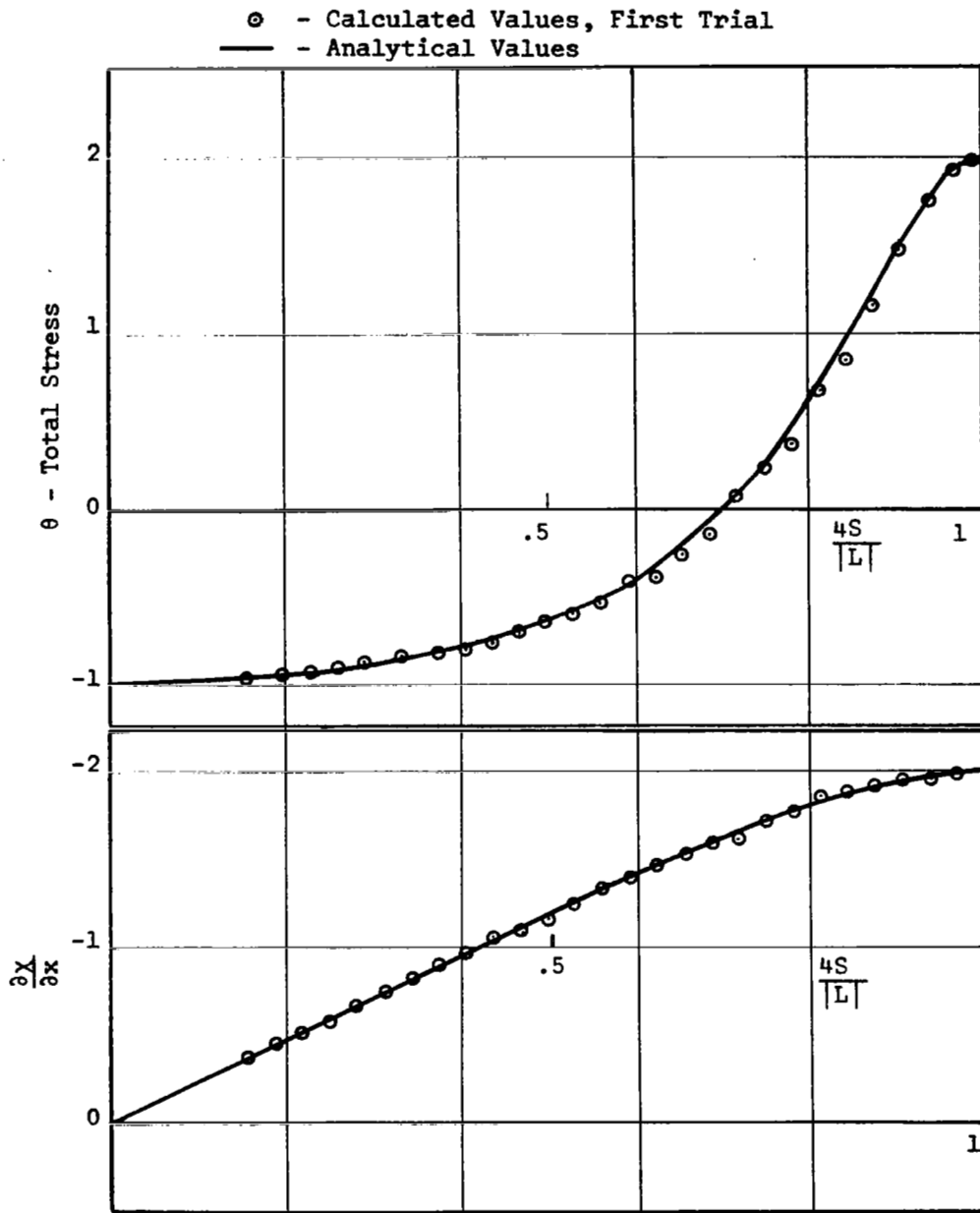


Figure 6. -Total stress and $\frac{\partial \theta}{\partial x}$ on the elliptic boundary,
 first trial, $a/b = 2$, $a = 2$.

The results in Figure 5 illustrate that the approximate stress function only crudely represents the exact stress function. However, consideration of these results lead to a quite profitable examination of the characteristics of the approximate solution. The results of this examination and subsequent improvements in the accuracy of the approximate stress function are discussed below.

Figure 6 shows calculated and analytical values of the total stress and $\frac{\partial \chi}{\partial x}$. The total stress depends on the source density $\sigma(s)$, not on $\mu(s)$. However, $\frac{\partial \chi}{\partial x}$ depends on both source density functions. The excellent agreement between the calculated and analytical values strongly implies that the source density functions used are accurate. However, further examination of the numerical results discloses that the procedure for determining the source density coefficients $t_{\sigma i}$, $v_{\sigma i}$, $t_{\mu i}$, and $v_{\mu i}$ from the specified end point values (σ_i and μ_i) causes considerable fluctuation in the slope of the approximate density functions. These fluctuations are not consistent with the appearance of the plotted values of the known source densities. They are introduced because conditioning of the known source densities values is required and because the coefficients $t_{\sigma i}$ and $t_{\mu i}$ depend on the difference of known values. Small inaccuracies in the known values become magnified and lead to considerable distortion in the first derivatives of the density functions with respect to s . Figure 7 shows a plot of the parameter $h \frac{d\rho^*}{ds}$ ($\rho = \sigma$ or μ) for the first trial at the problem. The significance of the fluctuations of the source density slopes is found in the comparison of $h \frac{d\mu}{ds}$ and the calculated values of τ_t .

It can be noted from Figures 5 and 7 that the relative extremums in the values of these two quantities correlate with one another. In comparing the two figures, it is possible to decide which values of $h \frac{d\rho}{ds}$ are high and which are low. The results of such a comparison is supported by calculations which show that the origin of the shear fluctuations are the terms with coefficient t_{i+1} in equation (31 e) for $H_{\eta\epsilon}^\rho$ when $\rho = \mu$. Note that there is much less fluctuation in $h \frac{d\sigma}{ds}$ than in $h \frac{d\mu}{ds}$ and also that the magnitude of $h \frac{d\sigma}{ds}$ is generally much less than $h \frac{d\mu}{ds}$ for $\frac{4s}{|L|} > .5$ so that the coefficients $t_{\sigma i}$ make only a small contribution to the shear fluctuations shown in Figure 5.

In addition to the information previously discussed, Figure 7 also shows the values of $t_{\sigma i}$ and $t_{\mu i}$ used in the final trial. A comparison between the source density values implied by these slopes and the known source density values is shown in Figure 8.

*Because boundary intervals of equal length h are chosen at interval end points, the parameter $h \frac{d\rho}{ds}$ is equal to $t_{\sigma i}$ when $\rho \equiv \sigma$ and $t_{\mu i}$ when $\rho \equiv \mu$.

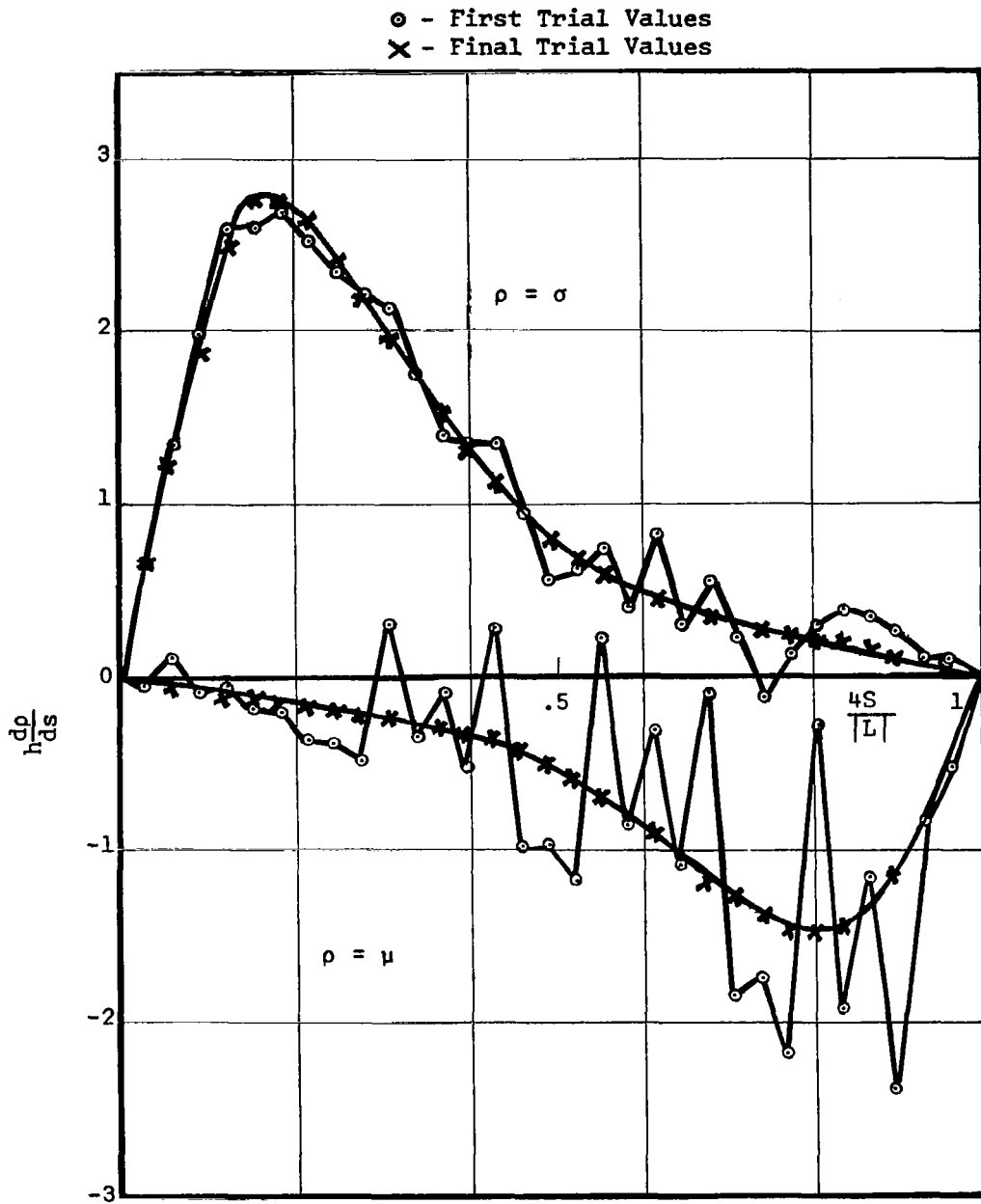


Figure 7. -First and final values of $\frac{dp}{ds}$, $a/b = 2$, $a = 2$.

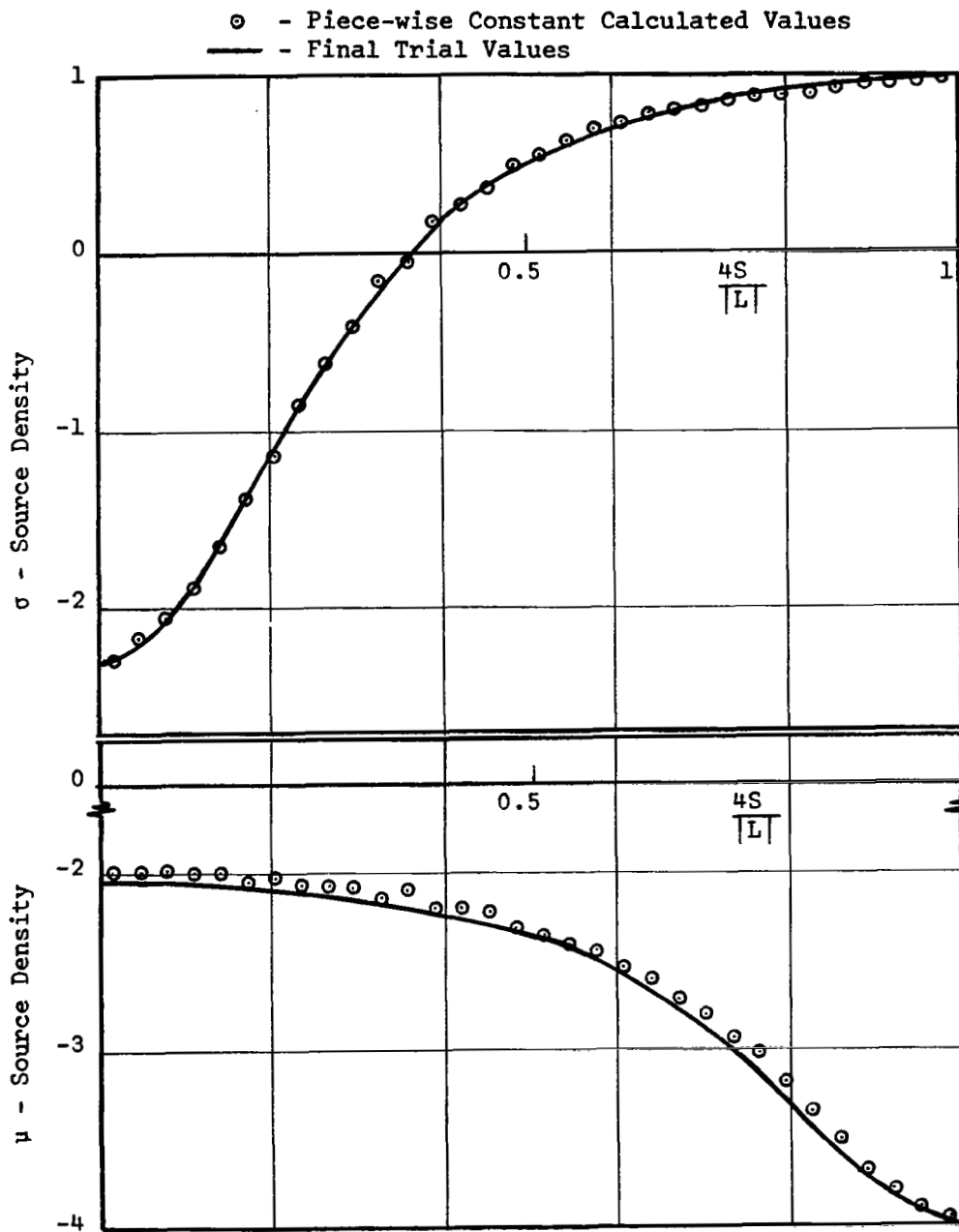


Figure 8. -Source density functions on the ellipse with $a/b = 2$, $a = 2$.

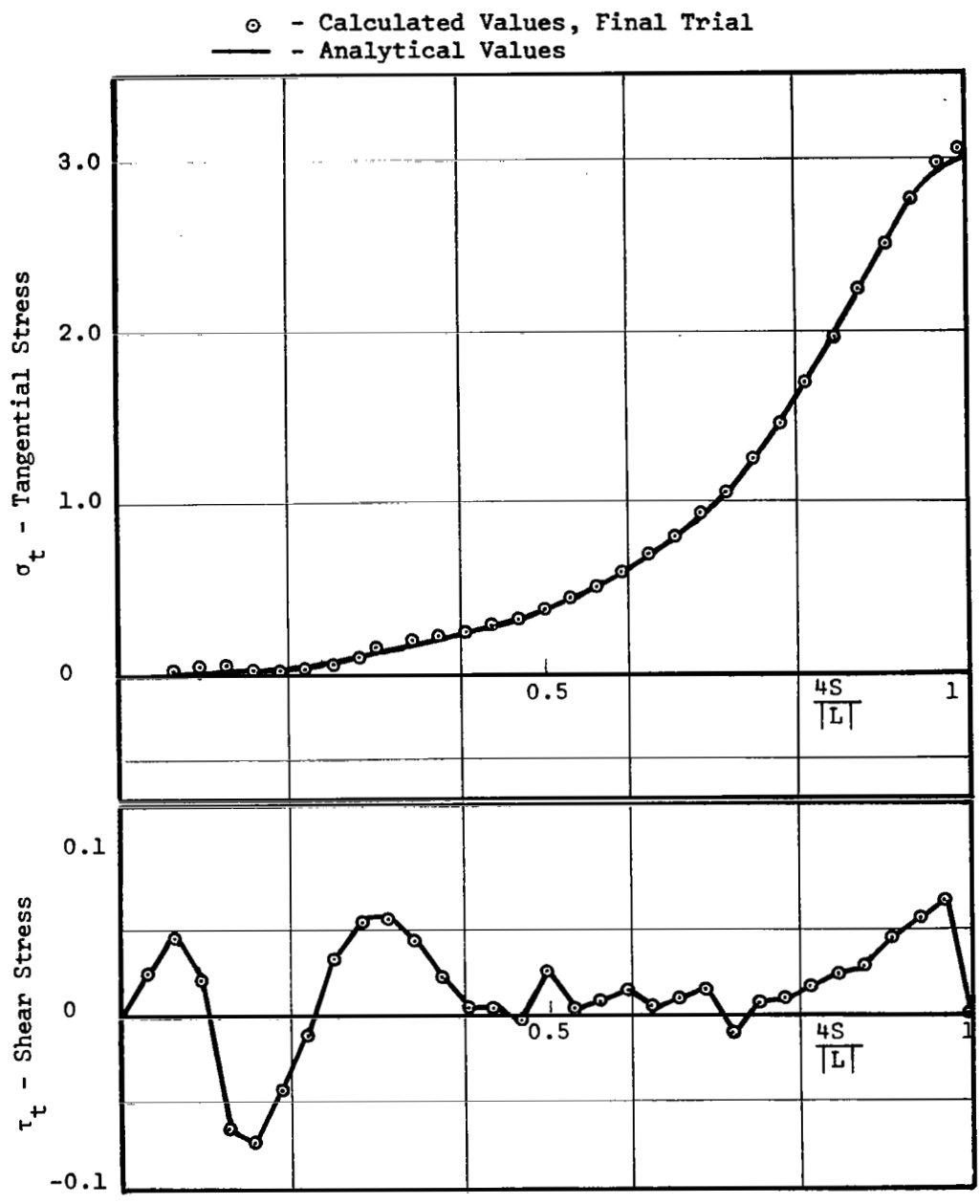


Figure 9. -Normal stress and shear stress tangent to the elliptic boundary, final trial, a/b = 2.

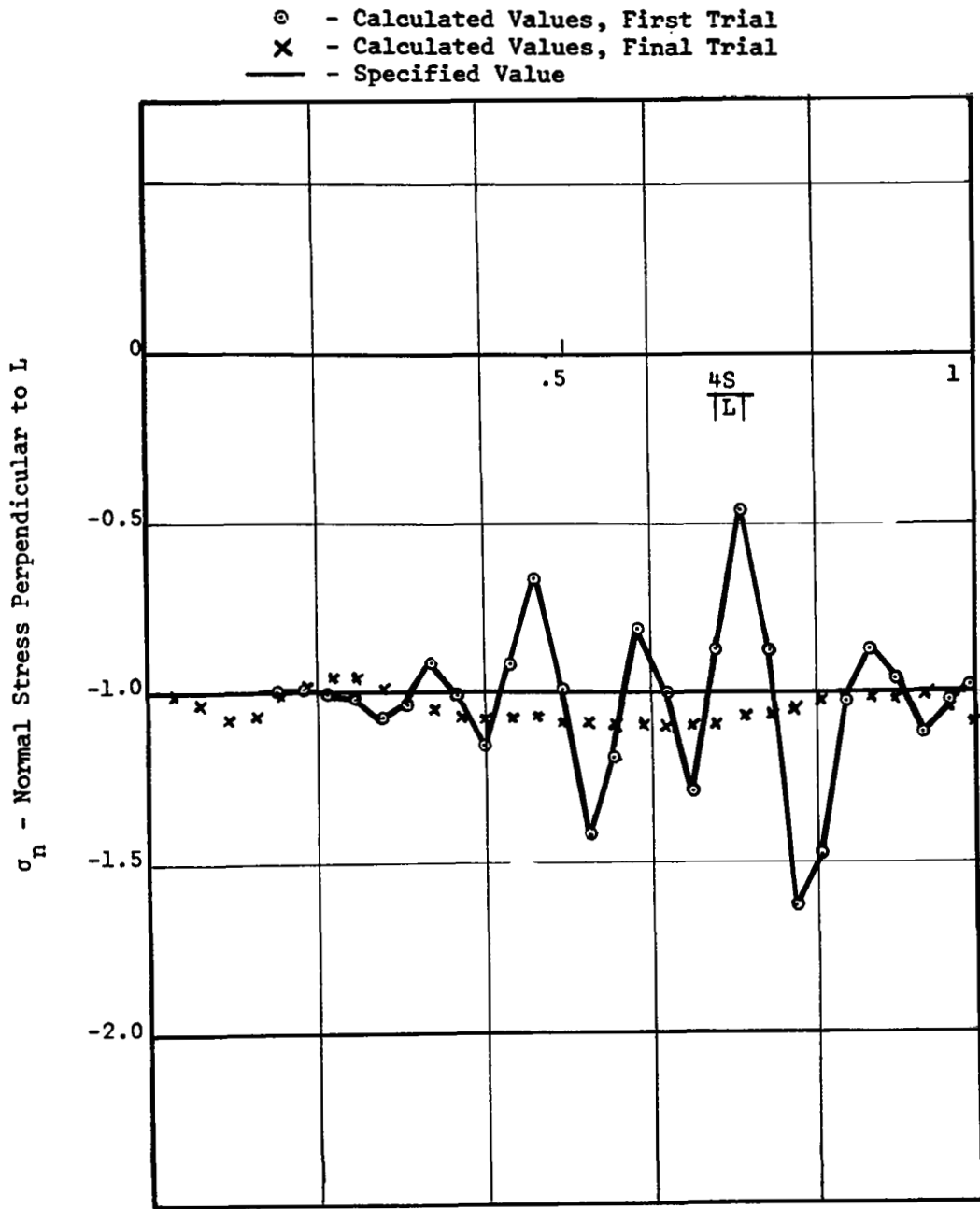


Figure 10. -Normal stress perpendicular to the elliptic boundary, $a/b = 2$.

For the final attempt at the problem of the elliptical hole with $a/b = 2$, source density functions with the properties given in Figures 7 and 8 were used. Calculated values of the tangential stress and shear stress components are shown in Figure 9. Analytical values are also shown. The results are excellent and show considerable improvement from those reported in Figure 5. Note that the computed values of shear stress are roughly an order of magnitude less than those shown in Figure 5. Also the adjustment in source density slopes gave considerable improvement in the accuracy of the computation for σ_t .

The final results presented for this example are given in Figure 10. Shown in this figure are the calculated values of the normal stress component, σ_n , perpendicular to the boundary. The value of this stress component is known to be -1 because of the specified boundary loading. Results are shown for both the first and final trials for the problems and indicate the same improvement noted with regard to the shear stress calculation. For the range $.4 < \frac{4s}{|L|} < .7$, the value of σ_n is nearly constant at -1.08. For this range of the parameter $\frac{4s}{|L|}$, Figure 9 shows that $|\tau_t|$ is less than .025, an excellent approximation to the specified boundary condition. The reason that the normal stress component stabilizes at -1.08 instead of -1.00 is indicated in Figure 8 where it can be seen that the values of μ used in the final trial are slightly greater than those determined by the numerical solution of the integral equations.

Discussion of Results for the Ellipse With $a/b = 5$

For the problem of the ellipse with $a/b = 5$ and $a = 1$, each quadrant was divided into 51 intervals. Near the intersections of the boundary with the x axis, the rapid rate of change of the boundary curvature made it necessary to use boundary intervals of decreasing length in order to obtain an adequate approximation to the boundary using circular arcs. Figure 11 shows the behavior of the source density functions for this problem. The solid curves represent the source densities used in performing the boundary stress calculation while the plotted points indicates the piece-wise constant values determined by the numerical solution of the integral equations. As before, the data is plotted in terms of $4s/|L|$, where $s = 0$ at $x = 0$ and $y = 0.2$, and $4s/|L| = 1$ at $x = 1$ and $y = 0$. Values of σ are not shown for $4s/|L| < .13$ as this density function decreases rapidly to -36 at $s = 0$.

Figures 12 and 13 show calculated and analytical values of the tangential stress, σ_t , and the total stress, θ , on the boundary. It can be seen that the results depict quite well that the stress concentration at $x = a$ and the stress variation around the boundary. In order to produce these results, it was again necessary to smooth the slopes of the source density functions. In this instance, however, the task was more difficult because, near $x = a$, derivatives of both density functions were nearly equal so that simultaneous and consistent adjustments in both functions were required.

Figure 14 shows the calculated values of the shear stress, τ_t , and the normal stress, σ_n . The values specified for these components due to the boundary

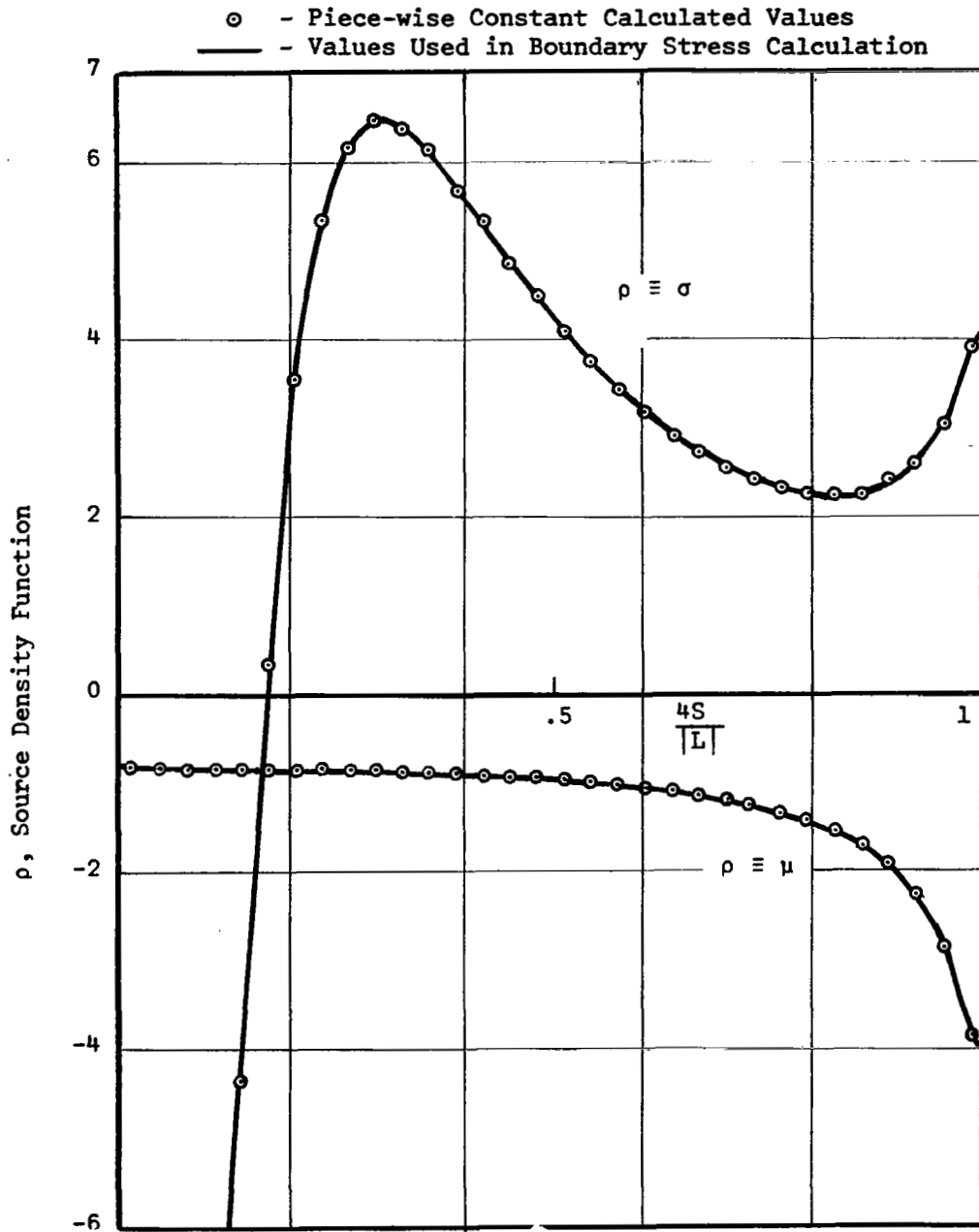


Figure 11. -Source density functions σ and μ , for the ellipse with $a/b = 5$, $a = 1$.

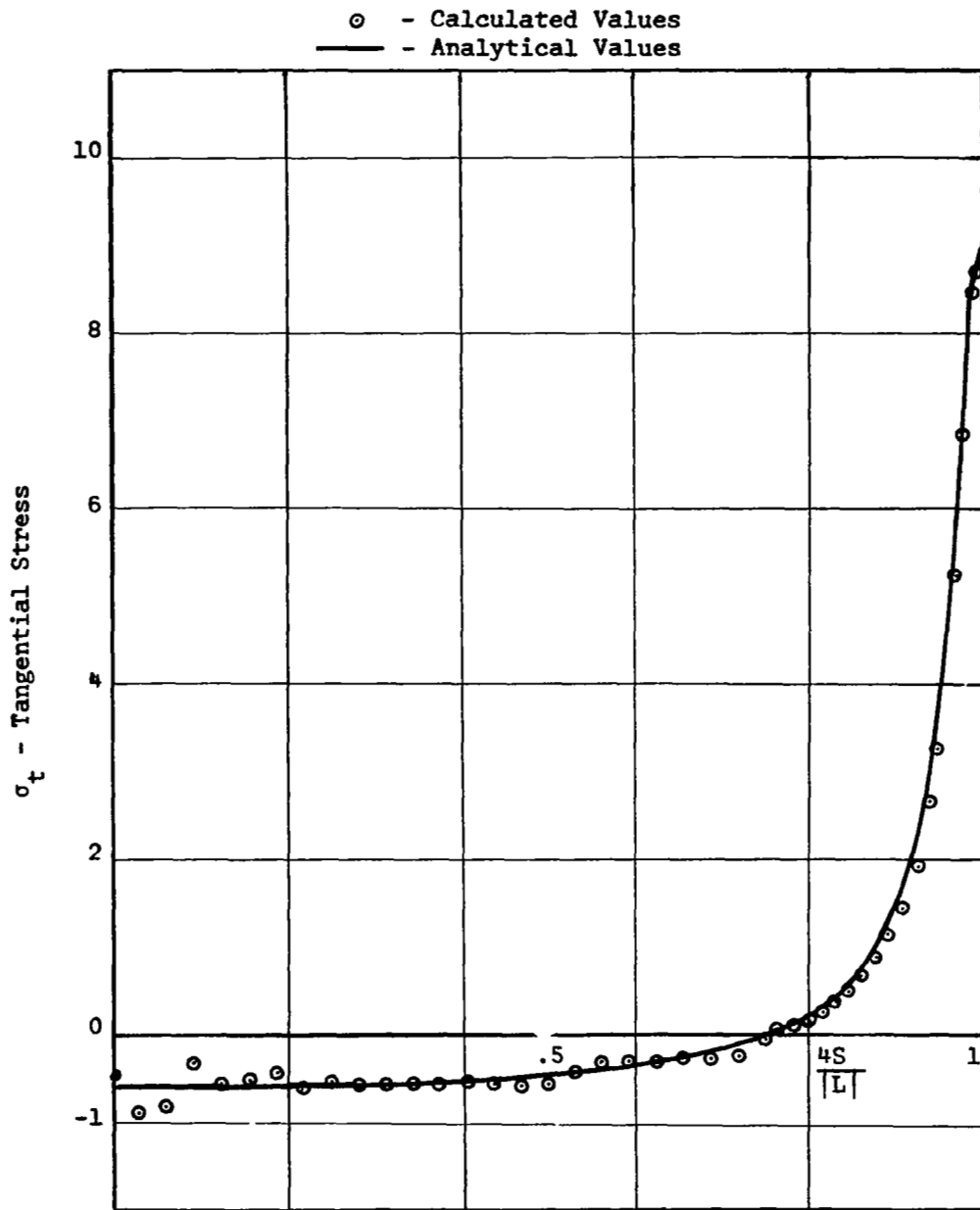


Figure 12. -Normal stress tangent to the elliptic boundary for $a/b = 5$.

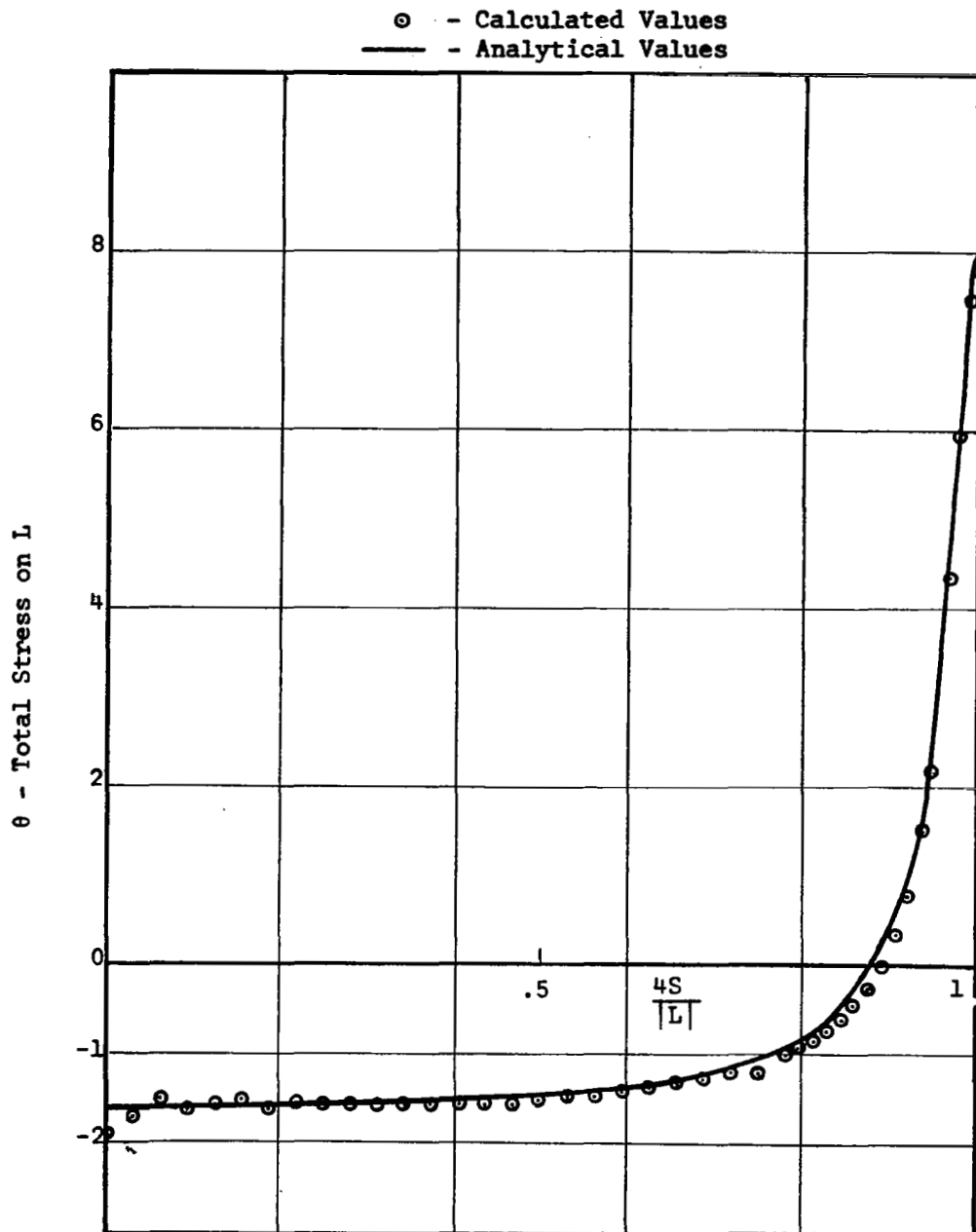


Figure 13. -Total stress on the elliptic boundary for $a/b = 5$.

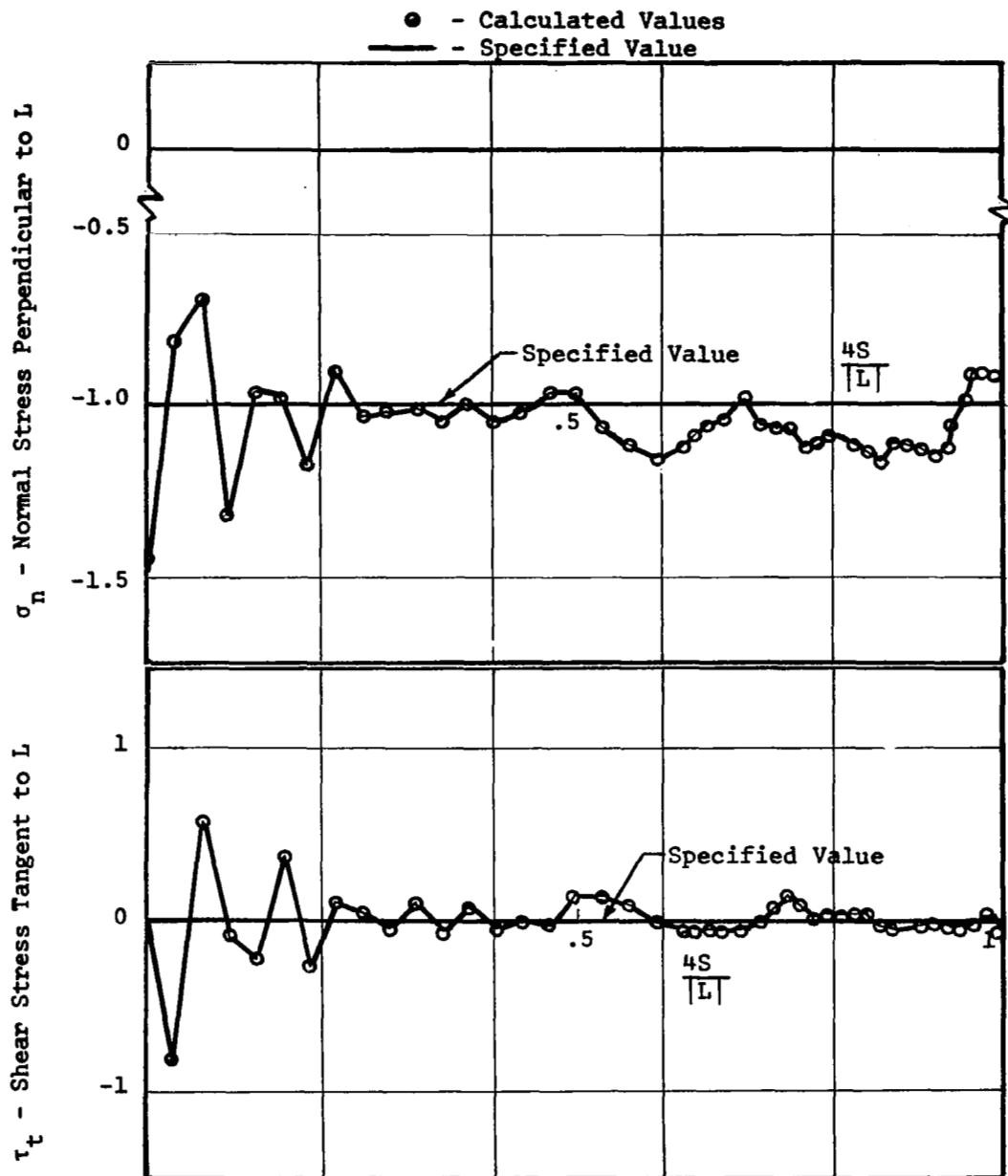


Figure 14. -Normal stress and shear stress at the elliptic boundary with $a/b = 5$.

loading are zero and -1 respectively. The difficulty in satisfying the boundary conditions near $s = 0$ is caused by the behavior of the source density $\sigma(s)$ in this area. No great effort was made to correct this situation as the stress pattern in this region is not of crucial importance.

Considerable effort was expended in making adjustments to the source density functions for $\frac{4s}{|L|} > .5$ in order to minimize the shear stress on the boundary. As shown in Figure 14, the results are excellent. Greater accuracy in the calculated values of σ_n would be desirable; however, the error is much less than the maximum tangential stress σ_t and does not create any significant distortions in the behavior of this stress component around the boundary. The results from this example indicate that the method and formulas used for calculating boundary stresses are accurate and are a valuable complement to the integral equation method given in (ref. 1).

General Comments on the Numerical Results

There are three comments of a general nature which relate to the numerical results presented in this section. First, results are presented for only one partitioning of the boundary for each example. Since a comparison between specified and calculated boundary tractions, rather than convergence, is the criterion for assessing the validity of a solution, there is no need to examine results from a series of boundary partitionings to decide which results are valid and which are of questionable reliability. However, in order to calculate boundary stresses accurately, it is necessary to make enough subdivisions of the boundary so that an adequate approximation of the boundary geometry is possible. The easiest way to insure that this goal has been accomplished by a particular partitioning is to construct a finer one and then to compare numerical results. Such a procedure was followed for both the numerical examples presented.

Second, it should be noted that the discrete values of the source densities determined as in (ref. 1) provide the basis for the source density functions used in the boundary stress calculation. Therefore, these discrete values should be determined with a view toward the subsequent boundary stress computation. That is, emphasis should be placed on determining a relatively high number of discrete values on those portions of the boundary where high stresses are expected. For example, it would be considerably simpler to obtain accurate results near $x = a$ for the ellipse problem ($a/b = 5$) if more source density values were known on this portion of the boundary.

The final comment relative to the numerical results presented are that they are by no means unique. In the course of obtaining the results presented for the second example, several slightly different specifications of the source densities near $x = a$ were used. Each represented a solution to a problem with slightly different boundary loading.

CONCLUDING REMARKS

The method presented for the direct computation of boundary stresses hinges directly on the determination of source density functions (satisfying the required continuity conditions) from discrete values of the source densities determined by the method outlined in (ref. 1). No standard or unique method for accomplishing this task has been developed; so the presentation of a direct, step-by-step, method for solving a given problem to within a specified accuracy is not yet available. However, the capability of calculating boundary stresses directly from an approximate stress function accomplishes at least two significant objectives. These include:

- 1) The attainment of good accuracy in approximate solutions on and close to the boundary through the use of more sophisticated representations of the source density functions.
- 2) The elimination of convergence as the criterion by which the accuracy of a numerical solution has been previously established. This feature is particularly important as it effectively removes the capability of computational machinery as a limitation on the applicability of the integral equation method.

A pertinent additional remark is that some of the ideas presented herein are applicable to harmonic problems (ref. 4) formulated and solved by a numerical method analogous to that presented in (ref. 1). Of particular significance is the idea of developing a more sophisticated source density representation based upon the discrete values of the source density. For harmonic problems, only the unknown function and its first derivatives are generally of interest on the boundary. Therefore, in order to be consistent with the physical situation, continuity in the one source density is only required. Here again a direct evaluation of the accuracy of the numerical solution through a comparison of computed and specified boundary quantities is possible and the necessity of using convergence as a criterion for accuracy can be eliminated.

The fundamental disadvantage of the method used to calculate boundary stresses is that there is no general method by which all the information required concerning the source density functions can be automatically generated. The data obtained by the method presented in (ref. 1) serves as a starting point. In general, a detailed examination of the characteristics of the approximate solution in regions of interest is required in order to attain acceptable accuracy.

APPENDIX A

DERIVATION OF LIMIT FORMULAS

The derivation of formulas for the limits given by (31) is outlined in this appendix. To obtain the expressions for H^{ρ} , H_{ϵ}^{ρ} , H_{η}^{ρ} , $H_{\epsilon\epsilon}^{\rho}$, and $H_{\eta\epsilon}^{\rho}$ given by (31), it is necessary to evaluate the limits in the equations

$$H^{\rho} = \lim_{\substack{\epsilon \rightarrow 0 \\ \eta = 0}} \bar{S}_{\rho} ,$$

$$H_{\epsilon}^{\rho} = \lim_{\substack{\epsilon \rightarrow 0 \\ \eta = 0}} \frac{\partial \bar{S}_{\rho}}{\partial \epsilon}$$

$$H_{\eta}^{\rho} = \lim_{\substack{\epsilon \rightarrow 0 \\ \eta = 0}} \frac{\partial \bar{S}_{\rho}}{\partial \eta} ,$$

$$H_{\epsilon\epsilon}^{\rho} = \lim_{\substack{\epsilon \rightarrow 0 \\ \eta = 0}} \frac{\partial^2 \bar{S}_{\rho}}{\partial \epsilon^2}$$

and

$$H_{\eta\epsilon}^{\rho} = \lim_{\substack{\epsilon \rightarrow 0 \\ \eta = 0}} \frac{\partial^2 \bar{S}_{\rho}}{\partial \epsilon \partial \eta}$$

(A.1 a-e)

where \bar{S}_{ρ} is given by equation (30).

The derivation of the required limits is aided by the use of two theorems from advanced calculus (ref. 7).

Theorem 1:

If $F(\epsilon) = \int_a^b f(\epsilon, \alpha) d\alpha$ and f is continuous for $a \leq \alpha \leq b$, $c \leq \epsilon \leq d$, then

$$\lim_{\epsilon \rightarrow \epsilon_0} F(\epsilon) = \int_a^b f(\epsilon_0, \alpha) d\alpha$$

if $c \leq \epsilon_0 \leq d$.

Theorem 2:

If $F(\epsilon) = \int_a^b f(\epsilon, \alpha) d\alpha$ and f and $\frac{\partial f}{\partial \epsilon}$ are continuous for $a \leq \alpha \leq b$ and $c \leq \epsilon \leq d$, then

$$F'(\epsilon) = \int_a^b \frac{\partial f}{\partial \epsilon} d\alpha .$$

A general result in potential theory (ref. 1) is that the single-layer potential is continuous onto the boundary. Hence, equation (31 a) for H^{ρ} is formed

simply by substituting $\epsilon = 0$ and $\eta = 0$ into (30) and defining the resulting expression to be H^p .

To establish the remainder of the formulas (31), first assume $\epsilon \geq \epsilon^* > 0$ so that Theorem 2 can be used to justify reversing the order of integration and differentiation. Then η is set equal to zero in the resulting integrals.

After these operations, one obtains

$$H_\epsilon^p = \lim_{\epsilon \rightarrow 0} \left[R_i \int_0^{\delta_i} \frac{\rho^i(\alpha) [R_i(1-\cos \alpha) + \epsilon] d\alpha}{D_i} \right. \\ \left. + R_{i+1} \int_0^{\delta_{i+1}} \frac{\rho^{i+1}(\alpha) [R_{i+1}(1-\cos \alpha) + \epsilon] d\alpha}{D_{i+1}} \right] \quad (A.2)$$

and

$$H_\eta^p = \lim_{\epsilon \rightarrow 0} \left[R_i^2 \int_0^{\delta_i} \frac{\rho^i(\alpha) \sin \alpha d\alpha}{D_i} \right. \\ \left. - R_{i+1}^2 \int_0^{\delta_{i+1}} \frac{\rho^{i+1}(\alpha) \sin \alpha d\alpha}{D_{i+1}} \right] , \quad (A.3)$$

where $D_i = 2(R_i^2 + \epsilon R_i)(1-\cos \alpha) + \epsilon^2$. The source density functions $\rho^i(\alpha)$ and $\rho^{i+1}(\alpha)$ are given by (26) and (27) and satisfy the continuity conditions given by (28) and (29). To evaluate the above limits, one first integrates over the range $0 \leq \alpha \leq \lambda$ where $\lambda < \min \{\delta_i, \delta_{i+1}\}$ is chosen small so that one may take $1-\cos \alpha \approx \alpha^2/2$ and $\sin \alpha \approx \alpha$. The resulting integrals may be evaluated analytically. Substituting the results into (A.2) and (A.3), passing to the limit in ϵ (using Theorem 2 where necessary) yields the following results:

$$H_\epsilon^p = \pi \rho_{i+1} + \lim_{\lambda \rightarrow 0} \left[\frac{1}{2} \int_\lambda^{\delta_i} \rho^i(\alpha) d\alpha + \frac{1}{2} \int_\lambda^{\delta_{i+1}} \rho^{i+1}(\alpha) d\alpha \right]$$

and

$$H_\eta^p = \frac{1}{2} \rho_{i+1} \log \frac{(1-\cos \delta_i)}{(1-\cos \delta_{i+1})} \\ + \lim_{\lambda \rightarrow 0} \left[\frac{1}{2} \delta_i^2 \int_\lambda^{\delta_i} \frac{[\alpha^2 v_i - \alpha \delta_i (t_i + 2v_i)] \sin \alpha d\alpha}{1-\cos \alpha} \right. \\ \left. - \frac{1}{2\delta_{i+1}^2} \int_\lambda^{\delta_{i+1}} \frac{[\alpha \delta_{i+1} t_{i+1} + \alpha^2 v_{i+1}] \sin \alpha d\alpha}{1-\cos \alpha} \right] .$$

The integrands above are continuous for $0 \leq \alpha \leq \delta_i$ and $0 \leq \alpha \leq \delta_{i+1}$, so the above expressions reduce directly to (31 b) and (31 c).

Reversing the order of integration and differentiation in (A.1 d) (justified by Theorem 2 for $\epsilon > 0$) and setting $\eta = 0$ gives the expression

$$\begin{aligned}
H_{\epsilon\epsilon}^{\rho} &= \rho_{i+1} \lim_{\epsilon \rightarrow 0} \left[\int_0^{\delta_i} G(\epsilon, R_i, \alpha) d\alpha + \int_0^{\delta_{i+1}} G(\epsilon, R_{i+1}, \alpha) d\alpha \right] \\
&+ \lim_{\epsilon \rightarrow 0} \left[\frac{t_{i+1}}{\delta_{i+1}} \int_0^{\delta_{i+1}} \alpha G_{i+1} d\alpha - \frac{(t_i + 2v_i)}{\delta_i} \int_0^{\delta_i} \alpha G_i d\alpha \right] \\
&+ \lim_{\epsilon \rightarrow 0} \left[\frac{v_i}{\delta_i^2} \int_0^{\delta_i} \alpha^2 G_i d\alpha + \frac{v_{i+1}}{\delta_{i+1}^2} \int_0^{\delta_{i+1}} \alpha^2 G_{i+1} d\alpha \right] \quad (A.4)
\end{aligned}$$

where

$$G(\epsilon, R_i, \alpha) = \frac{R_i [(2R_i^2 + 2\epsilon R_i)(1 - \cos \alpha) - 2(R_i(1 - \cos \alpha) + \epsilon)^2]}{[(2R_i^2 + 2\epsilon R_i)(1 - \cos \alpha) + \epsilon^2]^2} \equiv G_i \quad (A.5)$$

The limits in (A.4) are denoted by I_1 , I_2 , and I_3 respectively.

The integrals in the first limit, I_1 , can be evaluated analytically. Letting ϵ approach zero yields the result

$$I_1 = -\frac{1}{2} \left[\frac{\delta_i + \pi + \text{ctn} \frac{1}{2}\delta_i}{R_i} + \frac{\delta_{i+1} + \pi + \text{ctn} \frac{1}{2}\delta_{i+1}}{R_{i+1}} \right] \quad (A.6)$$

Note that I_2 can be rewritten as

$$\begin{aligned}
I_2 &= \frac{t_{i+1}}{\delta_{i+1}} \int_0^{\delta_{i+1}} G(0, R_{i+1}, \alpha) d\alpha \\
&+ \lim_{\epsilon \rightarrow 0} \int_0^{\delta_i} \alpha \left(\frac{t_{i+1}}{\delta_{i+1}} G(\epsilon, R_{i+1}, \alpha) - \frac{(t_i + 2v_i)}{\delta_i} G(\epsilon, R_i, \alpha) \right) d\alpha, \quad (A.7)
\end{aligned}$$

since G is continuous for $0 \leq \epsilon$ and $\delta_i \leq \alpha \leq \delta_{i+1}$ and hence Theorem 1 applies.

As

$$\frac{t_{i+1}}{R_{i+1} \delta_{i+1}} = \frac{(t_i + 2v_i)}{R_i \delta_i},$$

the limit in (A.7) can be written as

$$\bar{I}_2 = \frac{t_{i+1}}{R_{i+1} \delta_{i+1}} \lim_{\epsilon \rightarrow 0} \int_0^{\delta_i} \alpha [R_{i+1} G_{i+1} - R_i G_i] d\alpha. \quad (\text{A.8})$$

To evaluate \bar{I}_2 , one defines λ small ($\lambda > 0$) so that he can use $\cos \alpha \approx 1 - \alpha^2/2$, ($\lambda < \min\{\delta_i, \delta_{i+1}\}$). Then (A.5) becomes

$$\bar{G}(\epsilon, R_i, \alpha) = \frac{\alpha^2(R_i^2 - \epsilon R_i) - 2\epsilon^2 - \frac{1}{2}R_i^2 \alpha^4}{[(R_i^2 + \epsilon R_i)\alpha^2 + \epsilon^2]^2} = \bar{G}_i. \quad (\text{A.9})$$

The integral formed by substituting \bar{G}_i and \bar{G}_{i+1} into (A.8) and changing the upper limit to λ can be evaluated analytically. Then it can be shown that

$$\lim_{\epsilon \rightarrow 0} \int_0^\lambda \alpha [R_{i+1} \bar{G}_{i+1} - R_i \bar{G}_i] d\alpha = 0$$

independent of λ . Hence λ can be chosen as small as one pleases, justifying the approximation that $\cos \alpha = 1 - \alpha^2/2$. Since $\lambda > 0$, then by Theorem 1, \bar{I}_2 may be written as

$$\bar{I}_2 = \frac{t_{i+1}}{R_{i+1} \delta_{i+1}} \lim_{\lambda \rightarrow 0} \int_0^\lambda \alpha [R_{i+1} G(0, R_{i+1}, \alpha) - R_i G(0, R_i, \alpha)] d\alpha.$$

Now $G(0, R_i, \alpha) = \frac{\cos \alpha}{2R_i(1 - \cos \alpha)}$, so that the integrand above is identically zero.

Therefore $\bar{I}_2 \equiv 0$ and (A.7) reduces to

$$I_2 = \frac{t_{i+1}}{\delta_{i+1}} \int_{\delta_i}^{\delta_{i+1}} G(0, R_{i+1}, \alpha) d\alpha$$

or

$$I_2 = \frac{t_{i+1}}{2R_{i+1} \delta_{i+1}} \int_{\delta_i}^{\delta_{i+1}} \frac{\cos \alpha d\alpha}{(1 - \cos \alpha)}. \quad (\text{A.10})$$

Note that the coefficient $\frac{t_{i+1}}{R_{i+1} \delta_{i+1}}$ is simply the derivative of the source density function with respect to s at the common end-point of intervals i and $i+1$. The reduction of I_2 to the form given by (A.10) is not possible unless this derivative is continuous. If the derivative is discontinuous, the limit I_2 does not exist.

To evaluate I_3 , the third limit in (A.4), again one may introduce the angle $\lambda > 0$, use the approximation $\cos \alpha = 1 - \alpha^2/2$ and perform the indicated integration.

After letting ε approach zero, one finds that

$$I_3 = \frac{v_i}{\delta_i^2} \left(\frac{\lambda}{R_i} - \frac{\lambda^3}{6R_i^3} \right) + \frac{v_{i+1}}{\delta_{i+1}^2} \left(\frac{\lambda}{R_{i+1}} - \frac{\lambda^3}{6R_{i+1}^3} \right) \\ + \frac{v_i}{2\delta_i^2 R_i} \int_{\lambda}^{\delta_i} \frac{\alpha^2 \cos \alpha d\alpha}{1 - \cos \alpha} + \frac{v_{i+1}}{2R_{i+1} \delta_{i+1}^2} \int_{\lambda}^{\delta_{i+1}} \frac{\alpha^2 \cos \alpha d\alpha}{1 - \cos \alpha} .$$

Then $\lim_{\lambda \rightarrow 0} I_3$ reduces to the final result

$$I_3 = \frac{v_i}{2\delta_i^2 R_i} \int_0^{\delta_i} \frac{\alpha^2 \cos \alpha d\alpha}{1 - \cos \alpha} + \frac{v_{i+1}}{2R_{i+1} \delta_{i+1}^2} \int_0^{\delta_{i+1}} \frac{\alpha^2 \cos \alpha d\alpha}{1 - \cos \alpha} . \quad (A.11)$$

The derivation of formula (3ld) for $H_{\varepsilon\varepsilon}^0$ is now complete since by definition $H_{\varepsilon\varepsilon}^0 = \rho_{i+1} I_1 + I_2 + I_3$ and I_1 , I_2 , and I_3 are given by equations (A.6), (A.10) (A.11) respectively.

To obtain the limit formula for $H_{\eta\varepsilon}^0$, one may interchange the order of integration and differentiation in (A.1e) and, setting $\eta=0$, obtain

$$H_{\varepsilon\eta}^0 = \rho_{i+1} \lim_{\varepsilon \rightarrow 0} \left[\int_0^{\delta_{i+1}} F(\varepsilon, R_{i+1}, \alpha) d\alpha - \int_0^{\delta_i} F(\varepsilon, R_i, \alpha) d\alpha \right] \\ + \lim_{\varepsilon \rightarrow 0} \left[\frac{t_i + 2v_i}{\delta_i} \int_0^{\delta_i} \alpha F_i d\alpha - \frac{t_{i+1}}{\delta_{i+1}} \int_0^{\delta_{i+1}} \alpha F_{i+1} d\alpha \right] \\ + \lim_{\varepsilon \rightarrow 0} \left[\frac{v_{i+1}}{2\delta_{i+1}^2} \int_0^{\delta_{i+1}} \alpha^2 F_{i+1} d\alpha - \frac{v_i}{2\delta_i^2} \int_0^{\delta_i} \alpha^2 F_i d\alpha \right] \quad (A.12)$$

where

$$F(\varepsilon, R_i, \alpha) = \frac{+ 2R_i^2 \sin \alpha [R_i(1 - \cos \alpha) + \varepsilon]}{[(2R_i^2 + 2\varepsilon R_i)(1 - \cos \alpha) + \varepsilon^2]^2} = F_i . \quad (A.13)$$

Denote the limits appearing in (A.12) by J_1 , J_2 , and J_3 respectively:

$$H_{\varepsilon\eta}^0 = \rho_{i+1} J_1 + J_2 + J_3 , \quad (A.14)$$

The evaluation of limits J_2 and J_3 can be accomplished using the methods described to obtain the formula for $H_{\epsilon\epsilon}^{\rho}$. In order to evaluate J_2 , it is necessary to use the continuity condition on the derivative of the source density function. The limits J_2 and J_3 are given by

$$J_2 = \frac{\pi t_{i+1}}{R_{i+1} \delta_{i+1}} + \frac{1}{2} \frac{t_{i+1}}{R_{i+1} \delta_{i+1}} \left[\int_0^{\delta_i} \frac{\alpha \sin \alpha d\alpha}{1 - \cos \alpha} + \int_0^{\delta_{i+1}} \frac{\alpha \sin \alpha d\alpha}{(1 - \cos \alpha)} \right] \quad (\text{A.15})$$

and

$$J_3 = \frac{v_{i+1}}{2R_{i+1} \delta_{i+1}^2} \int_0^{\delta_{i+1}} \frac{\alpha^2 \sin \alpha d\alpha}{1 - \cos \alpha} - \frac{v_i}{2R_i \delta_i^2} \int_0^{\delta_i} \frac{\alpha^2 \sin \alpha d\alpha}{1 - \cos \alpha}. \quad (\text{A.16})$$

In attempting to evaluate J_1 , a difficulty is encountered. Formally, one can write

$$J_1 = \int_{\delta_i}^{\delta_{i+1}} F(0, R_{i+1}, \alpha) d\alpha + \lim_{\epsilon \rightarrow 0} \left[\int_0^{\delta_i} [F(\epsilon, R_{i+1}, \alpha) - F(\epsilon, R_i, \alpha)] d\alpha \right]. \quad (\text{A.17})$$

If the limit in (A.17) is denoted by \bar{J}_1 , performing the indicated integrations yields

$$\bar{J}_1 = \frac{1}{2} \frac{(R_i - R_{i+1})}{R_i R_{i+1}} \log(1 - \cos \delta_i) + \lim_{\epsilon \rightarrow 0} \left\{ \frac{1}{R_i} \log \frac{\epsilon}{R_i} - \frac{1}{R_{i+1}} \log \frac{\epsilon}{R_{i+1}} \right\}.$$

However, it is evident that the limit indicated above does not exist unless $R_i = R_{i+1}$, in which case $\bar{J}_1 = 0$. It is apparent that the source of the difficulty is the discontinuity in the boundary curvature artificially introduced by the use of tangent circular arcs to approximate the boundary contour.

A more detailed analysis of the contribution to $H_{\eta\epsilon}^{\rho}$ from the coefficient of ρ_{i+1} was performed using the assumption that the parametric equations in terms of s for the boundary contour could be expanded in a Taylor series about the point s_{i+1} over intervals i and $i+1$. The results indicated that the contribution to $H_{\eta\epsilon}^{\rho}$ was of the order of $(\min\{h_i, h_{i+1}\})^3$. Therefore, it was decided to neglect this contribution (effectively assuming $R_i = R_{i+1}$). In order to account for the dif-

ference in interval length, a term $r_i = (R_i + R_{i+1})/2$ was defined and J_1 was written as

$$J_1 = \int_{h_i/r_i}^{h_{i+1}/r_i} F(0, r_i, \alpha) d\alpha$$

or

$$J_1 = \frac{1}{r_i} \log \frac{(1 - \cos \frac{h_{i+1}}{r_i})}{(1 - \cos \frac{h_i}{r_i})} . \quad (\text{A.18})$$

This completes the discussion of $H_{\varepsilon\eta}^p$. Substitution of equations (A.15), (A.16), and (A.18) into (A.14) gives the formula (31e).

REFERENCES

1. Rim, K. and Henry, A. S., "An Integral Equation Method in Plane Elasticity," NASA Contractor Report, NASA CR-779, May 1967.
2. Symm, G. T., "Integral Equation Methods in Elasticity and Potential Theory," (PhD. Dissertation, University of London.), National Physical Laboratory, Mathematics Division, London, Dec. 1964.
3. Jaswon, M. A., Maiti, M., and Symm, G. T., "Numerical Biharmonic Analysis and Some Applications," Int. J. Solids Structures, Vol. 3, pp. 309-332, 1967, Pergamon Press Ltd.
4. Jaswon, M. A., "Integral Equation Methods in Potential Theory. I", Proc. Roy. Soc. Ser. A., Vol. 275, 1963, pp. 23-32.
5. Symm, G. T., "Integral Equation Methods in Potential Theory. II", Proc. Roy. Soc. Ser. A., Vol. 275, 1963, pp. 33-46.
6. Jaswon, M. A. and Ponter, A. R., "An Integral Equation Solution of the Torsion Problem," Proc. Roy. Soc. Ser. A., Vol. 273, 1963, pp. 237-246.
7. Buck, R. C., Advanced Calculus, International Series in Pure and Applied Mathematics, McGraw-Hill Book Company, Inc., New York, 1956.

FIRST CLASS MAIL

02U 001 57 01 BDS 69033 00903
AIR FORCE WEAPONS LABORATORY/AFWL/
KIRTLAND AIR FORCE BASE, NEW MEXICO 8711

ATT E. LOU BOWMAN, ACTING CHIEF TECH. LI

POSTMASTER: If Undeliverable (Section 158,
Postal Manual) Do Not Return

"The aeronautical and space activities of the United States shall be conducted so as to contribute . . . to the expansion of human knowledge of phenomena in the atmosphere and space. The Administration shall provide for the widest practicable and appropriate dissemination of information concerning its activities and the results thereof."

— NATIONAL AERONAUTICS AND SPACE ACT OF 1958

NASA SCIENTIFIC AND TECHNICAL PUBLICATIONS

TECHNICAL REPORTS: Scientific and technical information considered important, complete, and a lasting contribution to existing knowledge.

TECHNICAL NOTES: Information less broad in scope but nevertheless of importance as a contribution to existing knowledge.

TECHNICAL MEMORANDUMS: Information receiving limited distribution because of preliminary data, security classification, or other reasons.

CONTRACTOR REPORTS: Scientific and technical information generated under a NASA contract or grant and considered an important contribution to existing knowledge.

TECHNICAL TRANSLATIONS: Information published in a foreign language considered to merit NASA distribution in English.

SPECIAL PUBLICATIONS: Information derived from or of value to NASA activities. Publications include conference proceedings, monographs, data compilations, handbooks, sourcebooks, and special bibliographies.

TECHNOLOGY UTILIZATION PUBLICATIONS: Information on technology used by NASA that may be of particular interest in commercial and other non-aerospace applications. Publications include Tech Briefs, Technology Utilization Reports and Notes, and Technology Surveys.

Details on the availability of these publications may be obtained from:

SCIENTIFIC AND TECHNICAL INFORMATION DIVISION
NATIONAL AERONAUTICS AND SPACE ADMINISTRATION
Washington, D.C. 20546